

# Rocaglates convert DEAD-box protein eIF4A into a sequence-selective translational repressor

Shintaro Iwasaki<sup>1</sup>, Stephen N. Floor<sup>1</sup> & Nicholas T. Ingolia<sup>1</sup>

Rocaglamide A (RocA) typifies a class of protein synthesis inhibitors that selectively kill aneuploid tumour cells and repress translation of specific messenger RNAs<sup>1–4</sup>. RocA targets eukaryotic initiation factor 4A (eIF4A), an ATP-dependent DEAD-box RNA helicase; its messenger RNA selectivity is proposed to reflect highly structured 5' untranslated regions that depend strongly on eIF4A-mediated unwinding<sup>5</sup>. However, rocaglate treatment may not phenocopy the loss of eIF4A activity, as these drugs actually increase the affinity between eIF4A and RNA<sup>1,2,6</sup>. Here we show that secondary structure in 5' untranslated regions is only a minor determinant for RocA selectivity and that RocA does not repress translation by reducing eIF4A availability. Rather, *in vitro* and in cells, RocA specifically clamps eIF4A onto polypurine sequences in an ATP-independent manner. This artificially clamped eIF4A blocks 43S scanning, leading to premature, upstream translation initiation and reducing protein expression from transcripts bearing the RocA–eIF4A target sequence. In elucidating the mechanism of selective translation repression by this lead anti-cancer compound, we provide an example of a drug stabilizing sequence-selective RNA–protein interactions.

We analysed the global translational inhibition caused by RocA, as well as its marked messenger RNA (mRNA) selectivity, using ribosome profiling<sup>7</sup>. RocA treatment of HEK 293 cells caused a dose-dependent decrease in polysome formation and protein synthesis (Extended Data Figs 1a and 2a). Translation was inhibited without 4EBP dephosphorylation or eIF2 $\alpha$  phosphorylation (Extended Data Fig. 1b), but partly rescued by expression of RocA-resistant eIF4A proteins<sup>6</sup> (Extended Data Fig. 1c, d). We quantified the reduction in overall cytosolic ribosome footprints after normalization of our ribosome profiling data against footprints from the mitochondrial ribosome<sup>8</sup>, which employs molecular machinery distinct from the cytoplasmic translation apparatus (Fig. 1a and Extended Data Fig. 1e–h). We saw that RocA sensitivity varied widely across different transcripts (Fig. 1a, b and Supplementary Table 1a, b). This mRNA-specific translational repression occurred even at a low, therapeutically relevant concentration of RocA (30 nM)<sup>1–4</sup>, correlated well between different drug concentrations, and was not accompanied by significant changes in mRNA abundance (Extended Data Fig. 2b–d and Supplementary Table 1c).

Given that eIF4A acts during the scanning of the pre-initiation 43S complex along the 5' untranslated region (UTR)<sup>9</sup>, we reasoned that the varied RocA sensitivity of different mRNAs might be determined by their 5' UTR sequences. We confirmed that the 5' UTRs of selected mRNAs were sufficient to confer RocA sensitivity on a *Renilla* luciferase reporter, while the scanning-independent HCV IRES<sup>10</sup> was totally resistant to the drug (Fig. 1c and Extended Data Fig. 2e). However, RocA sensitivity did not reflect either the calculated thermodynamic stability or experimentally derived DMS-Seq secondary structure measurement<sup>11</sup> of the 5' UTR, and the presence of predicted G-quadruplexes<sup>5</sup> contributed only modestly (Extended Data Fig. 3).

Because RocA enhances the RNA affinity of eIF4A<sup>1,2,6</sup>, we suspected that it could induce effects beyond the simple loss of eIF4A activity.

Indeed, we found that the eIF4A inhibitor hippuristanol (Hipp), which decreases the affinity between eIF4A and RNA<sup>12,13</sup>, yields a different spectrum of mRNA-specific repression (Extended Data Fig. 4a–e). The mTOR inhibitor PP242, which inhibits formation of eIF4F (a complex of eIF4E/G/A)<sup>14,15</sup>, represses a subset of these Hipp-sensitive mRNAs (Extended Data Fig. 4f, g). Thus, RocA exerts effects beyond reduced eIF4A activity, particularly at low, therapeutic doses.

We next asked how RocA affected eIF4A occupancy across the transcriptome in cells by sequencing transcripts that co-purified with streptavidin binding peptide (SBP)-tagged eIF4A (Extended Data Fig. 5) (RNA-immunoprecipitation sequencing (RIP-seq)). Increasing

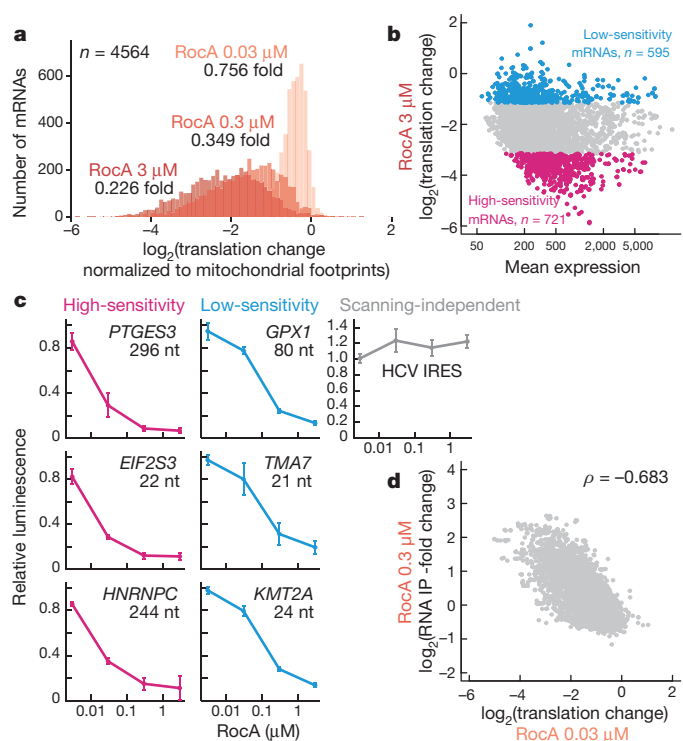


**Figure 1 | RNA sequence selectivity is imparted upon eIF4A by RocA causing selective translation repression.** **a**, Histogram of the number of transcripts along translation -fold change by ribosome profiling when cells are treated with 0.03, 0.3, or 3  $\mu$ M RocA, normalized to the number of mitochondrial footprints. Median -fold change is shown. Bin width is 0.1. **b**, MA plot of mean footprint reads between 3  $\mu$ M RocA treatment and non-treatment normalized to library sizes versus translation -fold change by 3  $\mu$ M RocA treatment, highlighting high- and low-sensitivity mRNAs. **c**, The 5' UTRs of indicated genes were fused to *Renilla* luciferase and these reporter mRNAs were transfected before treatment with RocA as indicated. Data represent mean and s.d. ( $n = 3$ ). **d**, Correlation of translation -fold change to RIP -fold change with RocA treatment.  $\rho$ , Spearman's rank correlation.

<sup>1</sup>Department of Molecular and Cell Biology, Center for RNA Systems Biology, University of California, Berkeley, California 94720, USA.

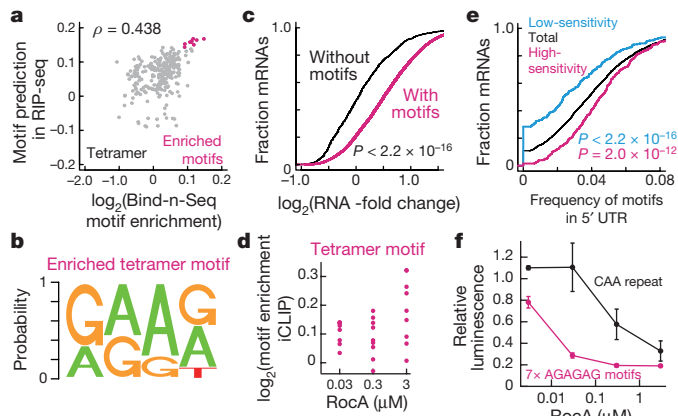


**Figure 2 | RNA Bind-n-Seq and iCLIP reveal that RocA preferentially increases the affinity between eIF4A and polypurine motif.**

**a**, Correlations between tetramer motif enrichment in Bind-n-Seq by  $0.03 \mu\text{M}$  RocA treatment and motif prediction of  $0.03 \mu\text{M}$  RocA effect in RIP-seq. **b**, Highest-scoring elements in Bind-n-Seq and RIP-seq. **c**, The change in mRNA binding for mRNAs with or without the enriched tetramer motif (**b**) in their 5' UTRs is shown as the RIP-fold change by RocA normalized to spike-in RNA. Significance is calculated by Mann–Whitney  $U$ -test. **d**, Enrichment of tetramer motifs (**b**) in iCLIP by RocA treatment relative to control dimethylsulfoxide (DMSO) treatment. **e**, The frequency of the tetramer motif (**b**) in the 5' UTR predicts whether a mRNA is high- or low-sensitivity, on the basis of the difference in cumulative distributions of motifs in the 5' UTR. Significance is calculated by Mann–Whitney  $U$ -test. **f**, Reporter assay in HEK 293 cells with a CAA-repeat 5' UTR containing seven polypurine motif (AGAGAG) insertions (Extended Data Fig. 9a). Data represent mean and s.d. ( $n = 3$ ).

RocA doses elevated the overall amount of RNA that co-purified with SBP-tagged eIF4A (Extended Data Fig. 5d), and greatly changed the abundance of individual transcripts, leading to 15-fold or larger differences between mRNAs. Strikingly, enhanced eIF4A binding in the presence of RocA correlated strongly with translation inhibition by RocA (Fig. 1d and Extended Data Fig. 5f), suggesting that a selective increase of the eIF4A–RNA affinity underlies the specific translation inhibition caused by RocA.

This mRNA selectivity led us to explore the sequence preferences of eIF4A in the absence and presence of RocA. We measured the RNAs that bound to eIF4A out of a random pool of oligonucleotides using deep sequencing (RNA Bind-n-Seq)<sup>16</sup> (Extended Data Fig. 6a–c). We then calculated the enrichment of 4- to 6-nucleotide (nt) motifs in RNAs retained on eIF4A, as DEAD-box RNA helicases typically contact 6 nt (ref. 17). The motifs enriched from randomized synthetic RNA by Bind-n-Seq also predicted RIP-seq enrichments of endogenous transcripts (Fig. 2a and Extended Data Fig. 6d). In both experiments, RocA greatly enhanced binding to short polypurine sequences (Fig. 2b, c and Extended Data Fig. 6e). Although drug-free eIF4A also had intrinsic RNA sequence preferences<sup>18</sup> (Extended Data Figs 6g) and transcripts containing these preferred sequences were relatively resistant to Hipp treatment (Extended Data Fig. 6h), RocA only selectively increases binding to a subset of sequences containing polypurine stretches (Extended Data Fig. 6g).

Polypurine motifs were also enriched in the eIF4A binding sites detected by photocrosslinking and immunoprecipitation (iCLIP)<sup>19</sup> after RocA treatment (Fig. 2d and Extended Data Fig. 7), and in the 5' UTRs of translationally RocA-sensitive mRNAs (Fig. 2e). This striking correspondence among *in vitro* binding to recombinant protein, *ex vivo* co-purification, crosslinking in cells, and translational repression in cells led us to hypothesize that selective binding to polypurine motifs induced by RocA binding could explain mRNA-specific translational repression. We then directly confirmed that inserting the polypurine motif into an unstructured CAA repeat 5' UTR (Extended Data Fig. 9a)<sup>20</sup> sensitized the reporter to RocA inhibition (Fig. 2f).

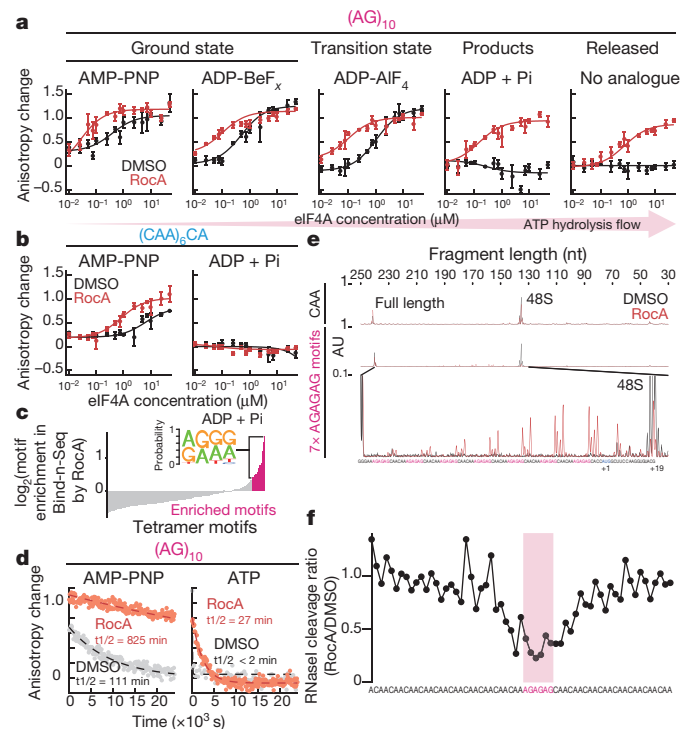


**Figure 3 | RocA clamps eIF4A on polypurine motif even after ATP hydrolysis.**

**a, b**, Direct measurement of the eIF4A/RNA affinity by fluorescence polarization for eIF4A and 5' FAM-labelled RNAs in the presence or absence of RocA. Data represent mean and s.d. ( $n = 3$ ). **c**, Motif enrichments along entire tetramer motifs in Bind-n-Seq with ADP + Pi and highest-scoring elements (inset). **d**, Competition assay with unlabelled RNA. Data represent mean ( $n = 3$ ). **e**, Ribosome toeprinting assay performed in RRL in the presence of GMP-PNP in the presence or absence of  $3 \mu\text{M}$  RocA treatment. **f**, Relative RNase I cleavage protected by eIF4A/RocA complex on mRNA containing one AGAGAG at the middle in footprinting assay. See the original data in Extended Data Fig. 9g.

We found that RocA-induced, sequence-selective eIF4A binding occurs through ATP-independent clamping that suffices to repress translation of the clamped mRNA. The cycle of ATP-dependent RNA binding and subsequent release upon ATP hydrolysis is necessary for the efficient RNA remodelling activity of eIF4A as well as its role in translation<sup>21</sup>. Drug-free eIF4A bound RNA only in the presence of ATP (AMP-PNP and ADP-BeF<sub>3</sub>) and transition state (ADP-AlF<sub>4</sub>) analogues but not hydrolysis products (ADP + Pi). Remarkably, RocA clamped eIF4A on polypurine RNA, but not CAA-repeat RNA, in an ATP-independent manner (Fig. 3a, b and Extended Data Fig. 8a, b). Bind-n-Seq performed with ADP + Pi likewise recovered polypurine-enriched RNAs in the presence of RocA and no detectable RNA in the absence of RocA (Fig. 3c and Extended Data Fig. 6i). RocA provided polypurine-specific RNA binding activity to mutant eIF4A defective for ATP binding (VX<sub>4</sub>GKT)<sup>22</sup>, which does not bind to RNA at all without RocA (Extended Data Fig. 8d–f), and even to the truncated amino (N)-terminal domain of eIF4A, albeit with lower affinity (Extended Data Fig. 8g). The eIF4A/RocA complex dissociated far more slowly from polypurine RNA than naive eIF4A, even in the presence of ATP, whose hydrolysis ordinarily permits rapid dissociation (Fig. 3d). High RNA affinity in the ADP-bound state can prolong RNA binding beyond the time required for adenosine nucleotide exchange to restore the high-affinity ATP-bound state and thus greatly reduce the effective dissociation rate. This effective dissociation rate from polypurine RNA measured in hydrolysable ATP (reflective of the intracellular environment) becomes much slower than the  $\sim 1$  min timescale of translation initiation<sup>23</sup>, and could serve to directly block the ribosome.

To probe how clamped eIF4A repressed translation, we recapitulated RocA-induced, polypurine motif-specific translational repression

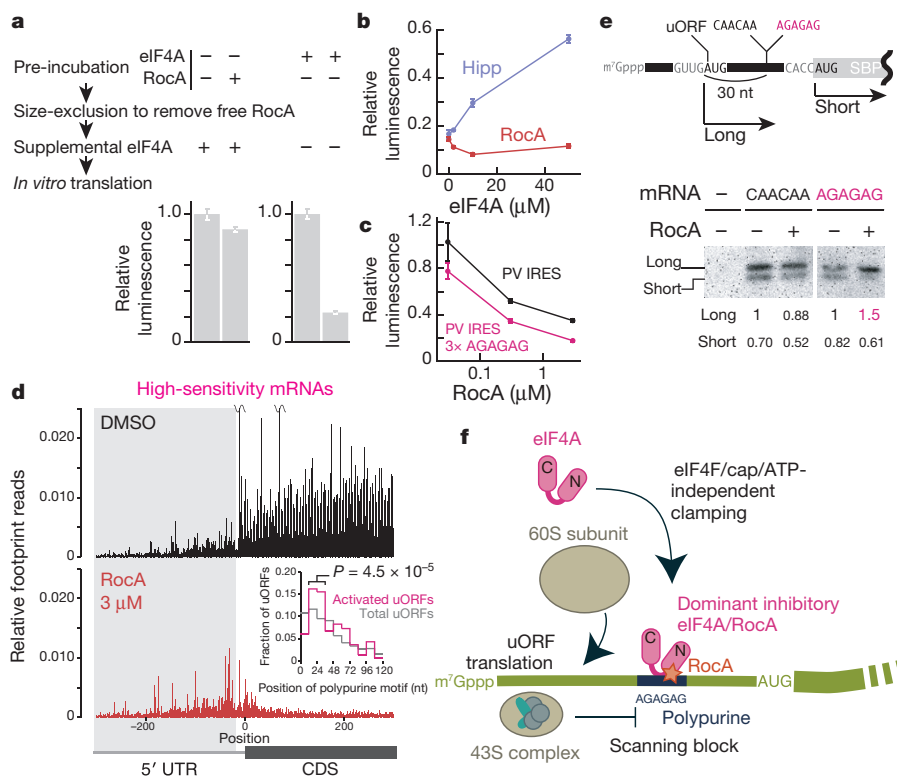


**Figure 4 | eIF4A/RocA complexes on polypurine motifs block scanning of pre-initiation complex, inducing uORF translation.** **a**, Pre-formation of the complex with RocA and eIF4A on the mRNA bearing seven polypurine motifs represses the translation from the mRNA in RRL. **b**, The supplementation of recombinant eIF4A protein to RRL *in vitro* translation reaction with 10  $\mu$ M Hipp or 3  $\mu$ M RocA. **c**, *In vitro* translation in RRL with mRNAs with native polio virus IRES and that with three polypurine motifs (Extended Data Fig. 9a). **d**, Meta-gene analysis of high-sensitivity transcripts to RocA. Reads are normalized to the sum of mitochondrial footprints reads. Histogram of the position of the first polypurine motif (hexamer) after uORF initiation codon (inset). *P* value is

in rabbit reticulocyte lysate (RRL) (Extended Data Fig. 9b, c). In this system, RocA treatment represses the formation of 48S pre-initiation complexes on the start codon of sensitive mRNAs, which we assessed using a primer extension toeprinting assay<sup>20,24</sup> (Fig. 3e and Extended Data Fig. 9d). Surprisingly, we observed additional RocA-dependent toeprints on the 5' UTR, corresponding to the position of polypurine motifs (Fig. 3e), even without eIF4F recruitment (Extended Data Fig. 9e). We recapitulated these toeprints using only purified eIF4A and drug, showing that they reflect eIF4A/RocA complexes clamped directly onto polypurine motifs, bypassing its canonical recruitment via cap and the eIF4F complex<sup>21</sup> (Extended Data Fig. 9f). RNase I footprinting revealed the full extent of the eIF4A protected region centred on the motif (Fig. 3f and Extended Data Fig. 9g).

These eIF4F-independent eIF4A/RocA complexes directly repress translation. We pre-formed such stable complexes on an mRNA during a pre-incubation with recombinant eIF4A and RocA, and then showed that they repressed its subsequent translation in the absence of free RocA (Fig. 4a). Recombinant forms of eIF4A bearing mutations that disrupt either ATP binding or eIF4G binding still retained the ability to clamp onto polypurine RNA in the presence of RocA (Extended Data Figs 8d–f, h, i and 9h–i) and repress translation from the RNA as strongly as wild-type eIF4A/RocA complex (Extended Data Fig. 9j). Furthermore, supplementation of recombinant eIF4A protein into an *in vitro* translation reaction actually strengthened the repressive effect of RocA (Fig. 4b and Extended Data Fig. 9k), confirming the dominant repressive effect of the eIF4A/RocA complex. In contrast, translation repression by Hipp, which decreases the affinity between

calculated by Fisher's exact test. Bin width is 12 nt. **e**, Western blot of SBP translated from uORF and downstream major ORF in RRL with 0.03  $\mu$ M RocA treatment. Quantification of bands normalized to long form with DMSO treatment is shown. For gel source data, see Supplementary Fig. 1. **f**, Schematic representation of RocA-mediated translation control. RocA clamps eIF4A onto mRNA by selective affinity enhancement for a polypurine motif in eIF4F-, cap-, and ATP-independent manners, which then blocks scanning of pre-initiation complex, introducing premature translation from uORF and inhibiting downstream ORF translation. In **b** and **c**, data represent mean and s.d. (*n* = 3).

RNA and thereby mimics a loss of its function, was relieved by the addition of recombinant eIF4A.

Assembly of an eIF4A/RocA complex could in principle repress 48S formation by blocking 40S attachment to the 5' end of an mRNA or subsequent 43S scanning along the 5' UTR. Because the impact of eIF4A/RocA bound to a single polypurine motif is unaffected by its distance from the 5' end (Extended Data Fig. 9a, l), we infer that eIF4A/RocA bound to these motifs blocks 43S scanning. We also found that eIF4A/RocA could inhibit translation from the polio virus internal ribosome entry site (IRES), which bypasses ordinary 40S recruitment but still depends on scanning (Extended Data Fig. 9a)<sup>25</sup> when we inserted polypurine motifs in the scanned region (Fig. 4c and Extended Data Fig. 9m). Scanning inhibition suffices to explain repression by the eIF4A/RocA complex, although our data do not exclude an additional effect on 40S loading.

Impediments to 43S scanning by stable hairpins<sup>26</sup> or RNA-binding proteins<sup>27</sup> can enhance the translation from upstream open reading frames (uORFs) that otherwise would be skipped. We observed that RocA treatment, but not Hipp treatment, caused an analogous accumulation of translation on 5' UTRs despite the global reduction in footprints on protein-coding sequences (CDSes) (Extended Data Fig. 10a, b). This enhancement occurred specifically on high-sensitivity transcripts (Fig. 4d and Extended Data Fig. 10c). The uORFs activated by RocA showed enrichment of a polypurine motif 20–30 nt downstream of the uORF initiation codon (Fig. 4d, inset), reflecting the distance between the start site and the leading edge of the scanning complex<sup>27</sup>. We tested directly whether eIF4A/RocA complexes on polypurine motifs

can drive cryptic upstream initiation using a reporter mRNA with two alternative start sites that yield distinguishable protein isoforms. Insertion of a polypurine motif 30 nt downstream of the earlier AUG increased translation initiation from this codon upon RocA treatment (Fig. 4e), confirming that clamped eIF4A/RocA complexes on polypurine motifs drive upstream translation initiation. We found evidence that this enhanced upstream initiation could contribute to eIF4A/RocA-mediated repression of downstream CDSes<sup>28</sup>, as RocA-sensitive transcripts showed more pre-existing uORF initiation<sup>29</sup> (Extended Data Fig. 10d, e).

We have shown that RocA induces ATP-independent clamping of eIF4A onto polypurine sequences, creating an inhibitory roadblock for the scanning ribosome (Fig. 4f). Our identification of the eIF4A/RocA binding motif provides the first observation of a drug that stabilizes sequence-selective RNA–protein interactions<sup>30</sup>. RocA may bind near the RNA interface on the N-terminal domain of eIF4A<sup>6</sup>, raising the possibility that the drug directly contacts purine bases of target RNAs. Alternatively, RocA might induce a conformational change leading to direct or indirect recognition of the polypurine motif by protein residues. Future structural insight into this polypurine selectivity may enable rocglate derivatives with altered base selectivities that target different mRNA.

**Online Content** Methods, along with any additional Extended Data display items and Source Data, are available in the online version of the paper; references unique to these sections appear only in the online paper.

Received 2 June 2015; accepted 5 April 2016.

Published online 15 June 2016.

- Cencic, R. *et al.* Antitumor activity and mechanism of action of the cyclopenta[*b*]benzofuran, silvestrol. *PLoS ONE* **4**, e5223 (2009).
- Bordeleau, M. E. *et al.* Therapeutic suppression of translation initiation modulates chemosensitivity in a mouse lymphoma model. *J. Clin. Invest.* **118**, 2651–2660 (2008).
- Liu, T. *et al.* Synthetic silvestrol analogues as potent and selective protein synthesis inhibitors. *J. Med. Chem.* **55**, 8859–8878 (2012).
- Santagata, S. *et al.* Tight coordination of protein translation and HSF1 activation supports the anabolic malignant state. *Science* **341**, 1238303 (2013).
- Wolfe, A. L. *et al.* RNA G-quadruplexes cause eIF4A-dependent oncogene translation in cancer. *Nature* **513**, 65–70 (2014).
- Sadlish, H. *et al.* Evidence for a functionally relevant rocglatamide binding site on the eIF4A-RNA complex. *ACS Chem. Biol.* **8**, 1519–1527 (2013).
- Ingolia, N. T., Ghaemmaghami, S., Newman, J. R. & Weissman, J. S. Genome-wide analysis *in vivo* of translation with nucleotide resolution using ribosome profiling. *Science* **324**, 218–223 (2009).
- Ingolia, N. T. *et al.* Ribosome profiling reveals pervasive translation outside of annotated protein-coding genes. *Cell Reports* **8**, 1365–1379 (2014).
- Sonenberg, N. & Hinnebusch, A. G. Regulation of translation initiation in eukaryotes: mechanisms and biological targets. *Cell* **136**, 731–745 (2009).
- Pestova, T. V., Shatsky, I. N., Fletcher, S. P., Jackson, R. J. & Hellen, C. U. A prokaryotic-like mode of cytoplasmic eukaryotic ribosome binding to the initiation codon during internal translation initiation of hepatitis C and classical swine fever virus RNAs. *Genes Dev.* **12**, 67–83 (1998).
- Rouskin, S., Zubradt, M., Washietl, S., Kellis, M. & Weissman, J. S. Genome-wide probing of RNA structure reveals active unfolding of mRNA structures *in vivo*. *Nature* **505**, 701–705 (2014).
- Bordeleau, M. E. *et al.* Functional characterization of IRESes by an inhibitor of the RNA helicase eIF4A. *Nature Chem. Biol.* **2**, 213–220 (2006).
- Lindqvist, L. *et al.* Selective pharmacological targeting of a DEAD box RNA helicase. *PLoS ONE* **3**, e1583 (2008).
- Hsieh, A. C. *et al.* The translational landscape of mTOR signalling steers cancer initiation and metastasis. *Nature* **485**, 55–61 (2012).
- Thoreen, C. C. *et al.* A unifying model for mTORC1-mediated regulation of mRNA translation. *Nature* **485**, 109–113 (2012).
- Lambert, N. *et al.* RNA Bind-n-Seq: quantitative assessment of the sequence and structural binding specificity of RNA binding proteins. *Mol. Cell* **54**, 887–900 (2014).
- Linder, P. & Jankowsky, E. From unwinding to clamping – the DEAD box RNA helicase family. *Nature Rev. Mol. Cell Biol.* **12**, 505–516 (2011).
- Abramson, R. D. *et al.* The ATP-dependent interaction of eukaryotic initiation factors with mRNA. *J. Biol. Chem.* **262**, 3826–3832 (1987).
- König, J. *et al.* iCLIP reveals the function of hnRNP particles in splicing at individual nucleotide resolution. *Nature Struct. Mol. Biol.* **17**, 909–915 (2010).
- Pestova, T. V. & Kolupaeva, V. G. The roles of individual eukaryotic translation initiation factors in ribosomal scanning and initiation codon selection. *Genes Dev.* **16**, 2906–2922 (2002).
- Parsyan, A. *et al.* mRNA helicases: the tacticians of translational control. *Nature Rev. Mol. Cell Biol.* **12**, 235–245 (2011).
- Pause, A. & Sonenberg, N. Mutational analysis of a DEAD box RNA helicase: the mammalian translation initiation factor eIF-4A. *EMBO J.* **11**, 2643–2654 (1992).
- Shah, P., Ding, Y., Niemczyk, M., Kudla, G. & Plotkin, J. B. Rate-limiting steps in yeast protein translation. *Cell* **153**, 1589–1601 (2013).
- Shirokikh, N. E. *et al.* Quantitative analysis of ribosome-mRNA complexes at different translation stages. *Nucleic Acids Res.* **38**, e15 (2010).
- Balvay, L., Soto Rifo, R., Ricci, E. P., Decimo, D. & Ohlmann, T. Structural and functional diversity of viral IRESes. *Biochim. Biophys. Acta* **1789**, 542–557 (2009).
- Kozak, M. Downstream secondary structure facilitates recognition of initiator codons by eukaryotic ribosomes. *Proc. Natl Acad. Sci. USA* **87**, 8301–8305 (1990).
- Medenbach, J., Seiler, M. & Hentze, M. W. Translational control via protein-regulated upstream open reading frames. *Cell* **145**, 902–913 (2011).
- Arribere, J. A. & Gilbert, W. V. Roles for transcript leaders in translation and mRNA decay revealed by transcript leader sequencing. *Genome Res.* **23**, 977–987 (2013).
- Lee, S. *et al.* Global mapping of translation initiation sites in mammalian cells at single-nucleotide resolution. *Proc. Natl Acad. Sci. USA* **109**, E2424–E2432 (2012).
- Pommier, Y. & Marchand, C. Interfacial inhibitors: targeting macromolecular complexes. *Nature Rev. Drug Discov.* **11**, 25–36 (2011).

Supplementary Information is available in the online version of the paper.

**Acknowledgements** We are grateful to J. Tanaka for providing hippuristanol, to Y. Tomari for sharing DNA constructs, to H. Asahara and University of California, Berkeley DNA sequencing facility for help with the toeprinting assay, and to A. Pinder and F. Tan for support with deep sequencing analysis. We also thank the members of Ingolia, Lareau, and Tomari laboratories for discussion and technical support. N.T.I. is a Damon-Runyon-Rachleff Innovator supported in part by the Damon Runyon Cancer Research Foundation (DRR-37-15), the Searle Scholars Program (11-SSP-229), and the National Institute of General Medical Sciences of the National Institutes of Health (P50GM102706). This work used the Vincent J. Coates Genomics Sequencing Laboratory at University of California, Berkeley, supported by National Institutes of Health S10 Instrumentation Grants S10RR029668, S10RR027303, and OD018174. S.I. is a recipient of Human Frontier Science Program long-term fellowship. S.N.F. is a Howard Hughes Medical Institute Fellow of the Helen Hay Whitney Foundation.

**Author Contributions** S.I. performed all experiments and analysed the data. Recombinant protein purification and the fluorescence polarization assay were performed with the help of S.N.F. S.I. and N.T.I. designed the experiments and wrote the manuscript.

**Author Information** Sequences generated in this study have been deposited in the Gene Expression Omnibus under accession numbers GSE70211 and GSE79392. Reprints and permissions information is available at [www.nature.com/reprints](http://www.nature.com/reprints). The authors declare no competing financial interests. Readers are welcome to comment on the online version of the paper. Correspondence and requests for materials should be addressed to N.T.I. ([ingolia@berkeley.edu](mailto:ingolia@berkeley.edu)).

## METHODS

No statistical methods were used to predetermine sample size. The experiments were not randomized. The investigators were not blinded to allocation during experiments and outcome assessment.

**General methods.** HEK 293 Flp-In T-Rex cells (Invitrogen) were cultured and recombined according to manufacturer's instructions. Stable integrants of SBP-tagged eIF4A were produced by co-transfection of these plasmids along with pOG44 by X-tremeGENE 9 (Roche) and selection using Hygromycin B. RocA, PP242, and thapsigargin were purchased from Sigma. Proteins and DNAs/RNAs were stained with GelCode Blue Stain Reagent (Thermo Scientific) and SYBR Gold Nucleic Acid Gel Stain (Invitrogen), respectively.

**Ribosome profiling.** Library preparation and data analysis were performed according to the method previously described<sup>31</sup>, which monitors mitochondrial ribosomes as well<sup>8,31</sup>. DMSO, RocA, Hipp, and PP242 were added to medium 30 min before cell lysis. The libraries were sequenced on a HiSeq 2000/2500 (Illumina).

**RIP-seq.** Cells with tetracycline-inducible, SBP-tagged eIF4A integrated stably were plated in a 10 cm dish and cultured for 3 days with  $1 \mu\text{g ml}^{-1}$  tetracycline, incubated with DMSO, 0.03  $\mu\text{M}$ , or 0.3  $\mu\text{M}$  RocA for 30 min, washed once with 5 ml of ice-cold PBS, lysed with 600  $\mu\text{l}$  of lysis buffer (20 mM Tris-HCl pH 7.4, 150 mM NaCl, 5 mM MgCl<sub>2</sub>, and 1 mM DTT) containing 1% Triton X-100 and Turbo DNase I (Invitrogen) 25 U ml<sup>-1</sup>, and then clarified by centrifugation for 10 min at 20,000g, 4°C. The supernatant was incubated with 60  $\mu\text{l}$  of Dynabeads M-270 Streptavidin (Invitrogen) equilibrated with lysis buffer containing 1% Triton X-100 at 4°C for 30 min. The beads were washed five times with lysis buffer containing 1% Triton X-100 and 1 M NaCl. SBP-eIF4A and bound RNAs were eluted with 25  $\mu\text{l}$  of lysis buffer containing 5 mM biotin at 4°C for 30 min. All buffers contained 0.001% DMSO with or without 0.03 or 0.3  $\mu\text{M}$  RocA. RNAs were extracted with QIAzol (Qiagen) using the Direct-zol RNA miniprep (Zymo Research). One-third of eluted RNA (~100 ng) was mixed with 1 ng of *in vitro* transcribed, spike-in *Renilla* luciferase RNA (*hRluc*) (see 'DNA constructs') and sequencing libraries were prepared using Tru-seq Ribo-zero gold kit (Illumina). Libraries were sequenced on HiSeq2000/2500 (Illumina) sequencers.

**iCLIP.** Cells were cultured as described in 'RIP-seq'. After medium was substituted with ice-cold PBS, the dishes on ice were irradiated with 150 mJ cm<sup>-2</sup> with UV-C (~254 nm) in UVP CL-1000 (UVP). Lysate was prepared as described in 'RIP-seq'. The lysate from a 10 cm dish (600  $\mu\text{l}$ ) was treated with 0.4 U of RNase I (Epicentre) at 37°C for 3 min. Reaction was quenched by the addition of 10  $\mu\text{l}$  of SUPERase In RNase Inhibitor (Invitrogen), and then incubated with 60  $\mu\text{l}$  of Dynabeads M-270 Streptavidin (Invitrogen) equilibrated with lysis buffer containing 1% Triton X-100 at 4°C for 30 min. The beads were washed by CLIP wash buffer (20 mM Tris-Cl pH 7.4, 1 M NaCl, 2 mM EDTA, 1 mM DTT, and 1% Triton X-100) twice, by CLIP wash buffer containing 0.1% SDS and 0.05% sodium deoxycholate twice, and then by lysis buffer containing 1% Triton X-100 twice. After discarding the supernatant, the beads were incubated with 10 U T4 PNK (NEB), 1  $\times$  PNK buffer, and 0.33  $\mu\text{M}$  <sup>32</sup>P- $\gamma$ [ATP] (3,000 Ci mmol<sup>-1</sup>, PerkinElmer) in 10  $\mu\text{l}$  at 37°C for 5 min and washed once with lysis buffer containing 1% Triton X-100. RNA-crosslinked proteins were eluted by 20  $\mu\text{l}$  of lysis buffer containing 1% Triton X-100 and 5 mM biotin at 37°C for 5 min, run onto NuPAGE (Invitrogen), and transferred to nitrocellulose membrane 0.45  $\mu\text{m}$  (Biorad). The images of <sup>32</sup>P-labelled RNA-protein complex on the membrane were acquired by Typhoon TRIO (Amersham Biosciences). The membrane with the region containing SBP-eIF4A/RNA complexes was excised and treated with 0.1  $\mu\text{g ml}^{-1}$  Proteinase K (Thermo Scientific), 200 mM Tris-Cl, pH 7.4, 25 mM EDTA, pH 8.0, 300 mM NaCl, and 2% SDS in 200  $\mu\text{l}$  at 55°C for 20 min. RNAs were isolated by phenol/chloroform extraction and ethanol precipitation. Library preparation was performed according to the method previously described<sup>31</sup> with the following modifications. As linker DNA, 5'-(Phos)NNNNNNIIITGATCGGAAGAGCACAGTCTGAA(ddC)-3', where (Phos) indicated 5' phosphorylation and (ddC) indicates a terminal 2', 3'-dideoxycytidine, was used. The capital letter Ns indicate random barcode and the letter Is indicate a sample multiplexing barcode. For multiplexing, linker DNAs containing ATCGT for DMSO replicate number 1, AGCTA for DMSO replicate number 2, CGTAA for RocA 0.03  $\mu\text{M}$ , CTAGA for RocA 0.3  $\mu\text{M}$ , and GATCA for RocA 3  $\mu\text{M}$  in I positions were used, respectively. The linker DNAs were pre-adenylated by 5' DNA adenylation kit (NEB) before the ligation reaction. Instead of gel extraction, unreacted linkers were removed by the treatment of the ligation reaction with 5' deadenylase (NEB) and RecJ exonuclease (Epicentre) at 30°C for 45 min. Reverse transcription was performed with an oligonucleotide 5'-(Phos)NNAGATCGGAAGAGCGTCTGTAGGGAAAGAG(iSp18)GTGACTGGAGTTCAGACGTGTGCTC-3', where (Phos) indicates 5' phosphorylation and Ns indicate random barcode. PCR was performed with oligonucleotides, 5'-AATGATACGGCGACCACCGAGATCTACACTCTTTCC

TACACGACGCTC-3' and 5'-CAAGCAGAAGACGGCATAACGAGATCGT GATGTGACTGGAGTTCAGACGTGTG-3'. Libraries were sequenced on HiSeq4000 (Illumina) sequencers. Random barcode was used to eliminate PCR duplicates in the library.

**Bind-n-Seq.** SBP-tagged eIF4A was purified as described in 'RIP-seq', without DMSO or RocA treatment. The beads tethering SBP-eIF4A were treated with 1  $\times$  Micrococcal Nuclease Buffer (NEB), 0.5  $\times$  lysis buffer, 0.5% Triton X-100, and 200 U  $\mu\text{l}^{-1}$  Micrococcal Nuclease (NEB) in 30  $\mu\text{l}$  at 25°C for 30 min, washed five times with lysis buffer containing 1% Triton X-100, 1 M NaCl, and 5 mM EGTA pH 7.4, and rinsed twice with lysis buffer containing 0.1% Triton X-100. The beads were incubated in lysis buffer containing 0.1% Triton X-100, 2 mM AMP-PNP, 0.33 U  $\mu\text{l}^{-1}$  SUPERase In RNase Inhibitor (Invitrogen), 1  $\mu\text{M}$  N<sub>30</sub> RNA ((N)<sub>30</sub>CTGTAGGACCATCAAT, where letters in bold type represent DNA sequence for reverse transcription primer hybridization) in 30  $\mu\text{l}$  at 37°C for 30 min, and washed five times with lysis buffer containing 0.1% Triton X-100, 2 mM AMP-PNP, and 0.1% DMSO. SBP-eIF4A/RNA complex was eluted with 30  $\mu\text{l}$  of lysis buffer containing 0.1% Triton X-100, 2 mM AMP-PNP, and 5 mM biotin. DMSO (0.1%) with or without 30 or 300 nM RocA was present in all buffers during the RNA binding reaction, wash, and elution. RNAs were extracted with QIAzol (Qiagen) using the Direct-zol RNA miniprep (Zymo Research) and converted into DNA library as the same method of ribosome profiling<sup>31</sup>. For Bind-n-Seq with ADP + Pi, 2 mM ADP, 2 mM Na<sub>2</sub>HPO<sub>4</sub>, 50  $\mu\text{M}$  N<sub>30</sub> RNA, and 3  $\mu\text{M}$  RocA were used.

The 30-nt randomized RNA followed by 3' DNA sequence for reverse transcription priming was designed to avoid ligation biases and sequencing of contaminating RNA fragments from cells during SBP-eIF4A purification, and to cover the entire sequence with a single 50-bp mode of HiSeq (Illumina) sequencers.

Our read depth (~10<sup>8</sup> reads) is less than the theoretical complexity (4<sup>30</sup> ≈ 10<sup>18</sup>), so that the probability that the same sequence appears multiple times in the library is quite low. Therefore, we assumed that reads with exactly the same sequence and length in the library reflect PCR duplicates and counted them only once. Motif enrichment in the range of interest (4–6 nt) was calculated as the ratio of the motif frequency between libraries<sup>16</sup>.

Spearman's correlation of motif number in 5' UTR versus RIP-seq -fold change caused by RocA treatment was used as motif prediction in RIP-seq. High-scoring motifs were defined as those with enrichment of the prediction or the enrichment is >1.5 s.d. from the mean in RIP-seq and Bind-n-Seq, respectively.

**Data analysis.** The reads were aligned to the hg19 human genome reference and the resulting aligned reads were mapped to University of California, Santa Cruz (UCSC) known reference genes, downloaded from the UCSC genome browser in July 2013. A UCSC bed file of known genes was used for the 5' UTR analysis. For mitochondrial footprints alignments, we used the RefSeq genes track corresponding to the mitochondrial chromosome (chrM), downloaded from UCSC genome browser. Specific A-site nucleotides were empirically estimated on the basis of the length of each footprint. The offsets were 14 for 26–29 nt and 15 for 30–31 nt. For mitochondria footprints, they were 9 for 26–27 nt, 11 for 28–29 nt, 12 for 30 nt, 13 for 31 nt, and 18 for 32–34 nt. For mRNA fragments, we used offset 14. For measuring footprint density and mRNA fragments of RIP-seq between samples, we restricted our analysis to genes, which have at least 40 and 100 summed counts in each sample, respectively. For CDSs, the analysis only included the transcript positions beginning 15 codons following the start codon and stopping 5 codons preceding the stop codon. For 5' UTRs, we included the transcript positions from the 5' end of the mRNA until 5 codons preceding the start codon. DESeq<sup>32</sup> was used to calculate relative enrichment of genes in the library, including the mitochondrial footprints and spike-in *hRluc* mRNA counts. The calculated -fold change was re-normalized to the value of the summed mitochondria footprints or the spike-in *hRluc* mRNA fragments.

High-sensitivity messages were defined as transcripts with reduction more than twofold from the median, and with *q* value < 0.01, between 3  $\mu\text{M}$  RocA-treated and untreated cells. Low-sensitivity transcripts are defined as same as high-sensitivity but with accumulation over twofold.

For calculation of  $\Delta G$ , RNALfold (ViennaRNA Package)<sup>33</sup> was run with -L30 -g options on 5' UTR sequences from UCSC foldUtr5 table. The minimum  $\Delta G$  along each 5' UTR was used as a representative free energy value for each gene.

The presence of G-quadruplexes was predicted with RNAfold (ViennaRNA Package).

The Gini differences across 5' UTRs were calculated using published data<sup>11</sup>. Analysis was restricted to the mRNAs bearing 5' UTRs having one or more reads on A/C positions on average.

'uORF translation intensity' was calculated using published data<sup>29</sup>. To incorporate the number and intensity of each upstream initiation site in the 5' UTR, we calculated the density of 5' UTR footprints for each transcript as mentioned

above, as the great majority of these footprints derive from ribosomes trapped on first codons (Extended Data Fig. 10d). To normalize mRNA abundance in cells, we normalized the density by footprint counts from the CDS start codon region using the genomic position between start codon and 6 nt downstream. We restricted the analysis to transcripts with at least ten counts from CDS start codons and re-normalized the value to the median as one.

**Code availability.** Scripts to run the analyses mentioned above are available upon request.

**Fluorescence polarization assay.** Proteins (0–50  $\mu$ M) were incubated in 14.4 mM HEPES-NaOH, 108 mM NaCl, 1 mM MgCl<sub>2</sub>, 0.36 mM TCEP, 14.4% glycerol, 0.1% DMSO, and 10 nM 5' FAM-labelled RNA with or without 50  $\mu$ M RocA in 10  $\mu$ l reaction for 30 min at 25 °C. The experiments were performed with 1 mM AMP-PNP (for AMP-PNP), 1 mM ADP, 5 mM BeCl<sub>2</sub>, and 25 mM NaF (for ADP-BeF<sub>3</sub>), 1 mM ADP, 5 mM AlCl<sub>3</sub>, and 25 mM NaF (for ADP-AlF<sub>4</sub>), or 1 mM ADP and 1 mM Na<sub>2</sub>HPO<sub>4</sub> (for ADP + Pi). For the condition without ATP analogue, MgCl<sub>2</sub> was omitted from the reaction.

For competition assay, the complexes were preformed with 1 mM ATP or AMP-PNP, 1  $\mu$ M eIF4A, 10 nM FAM-labelled RNA, and 50  $\mu$ M RocA and chased with 100  $\mu$ M non-labelled RNA. Because of the low affinity, 50  $\mu$ M eIF4A was used with ATP and DMSO.

Fluorescence polarization was measured using an Infinite F-200 PRO (TECAN). The dissociation constant ( $K_d$ ) and half-life ( $t_{1/2}$ ) were calculated with fitting to the Hill equation and one-phase exponential decay equation, respectively, by Igor Pro software (WaveMetrics).

**In vitro translation and toeprinting assay.** *In vitro* translation was performed with nuclease-treated RRL system (Promega), according to the manufacturer's instructions. Reporter mRNAs (50 nM; see 'DNA constructs') was incubated in 50% RRL with RocA (concentration shown in the figure legends) or 1% DMSO in 10  $\mu$ l at 30 °C for 1 h. For the detection of SBP, 20  $\mu$ l of the reaction was used with uORF + CAACAA or uORF + AGAGAG mRNAs and concentrated with 10  $\mu$ l of Dynabeads M-270 Streptavidin (Invitrogen).

The toeprinting assay was performed as previously described<sup>34</sup>. The reaction was pre-incubated with RRL in the presence of 2 mM GMP-PNP or m<sup>7</sup>GTP and 3  $\mu$ M RocA or 1% DMSO at 30 °C for 5 min, and then incubated with 50 nM mRNAs at 30 °C for 5 min, followed by reverse transcription with 10 U  $\mu$ l<sup>-1</sup> ProtoScript II (NEB) with 250 nM 5' 6'-FAM labelled primer (5'-6'-FAM-ATGCAGAAAAATCACGGC-3') at 30 °C for 15 min. Recombinant eIF4A (10  $\mu$ M) was used instead of RRL in 30 mM HEPES, pH 7.3, 100 mM KOAc, 1 mM Mg(OAc)<sub>2</sub>, and 1 mM DTT in the presence or absence of 10  $\mu$ M RocA. Complementary DNA (cDNA) was purified by phenol extraction, concentrated using Oligo Clean & Concentrator (Zymo Research), and run with GeneScan 600 LIZ Size Standard v2.0 (Life Technologies) on a 3730 DNA Analyzer (Life Technologies). Data were analysed by GeneMapper software (Life Technologies). For pre-formation of eIF4A/RocA complex on mRNA, 30  $\mu$ l of the reaction was loaded on G-25 column equilibrated with 30 mM HEPES, pH 7.3, 100 mM KOAc, 1 mM Mg(OAc)<sub>2</sub>, and 1 mM DTT to remove free RocA. The flow-through mRNA was used for *in vitro* translation at 20 nM.

Dideoxy-terminated sequencing of RNA was performed by reverse transcriptions using 0.125 mM individual dideoxy-NTP and 0.5 mM each deoxy-NTP with the same 5' 6'-FAM-labelled primer and ProtoScript II, according to the manufacturer's instructions.

**RNase I footprinting assay.** Reporter RNA was incubated with recombinant eIF4A and RocA in 12  $\mu$ l as described for the toeprinting assay. The reaction was treated with 1  $\mu$ l of 0.001 U  $\mu$ l<sup>-1</sup> RNase I (Epicentere) at room temperature for 5 min. After quenching the digestion by the addition of 1  $\mu$ l of SUPERase In RNase Inhibitor (Invitrogen), RNA was extracted by Oligo Clean & Concentrator (Zymo Research) and reverse transcribed by ProtoScript II (NEB) with 5' 6'-FAM labelled primer (5'-6'-FAM-ATGCAGAAAAATCACGGC-3') according to the manufacturer's instructions. The cDNA was run on 3730 DNA Analyzer (Life Technologies) as described for the toeprinting assay. Data were analysed by GeneMapper software (Life Technologies).

**Polysome profiling.** Cell lysate was prepared as described previously<sup>31</sup>. Lysate containing 15  $\mu$ g total RNA was loaded on to 10–50% linear sucrose gradients containing 20 mM Tris-HCl, pH 7.4, 150 mM NaCl, 5 mM MgCl<sub>2</sub>, 1 mM DTT, 100  $\mu$ g ml<sup>-1</sup> cycloheximide, and 2 U ml<sup>-1</sup> SUPERase In RNase Inhibitor and sedimented by ultracentrifugation at 220,000g for 2 h at 4 °C with an SW41 rotor (Beckman Coulter). Gradients were fractionated using Gradient station (Biocomp). Ultraviolet absorbance was detected by ECONO UV monitor (Biorad).

**Metabolic labelling of nascent peptide by OP-puro.** Nascent peptides in HEK 293 cells were labelled by 40  $\mu$ M OP-puro (Jena Bioscience) in 24-well dishes with 0–3  $\mu$ M RocA for 30 min. Cells were washed with PBS and lysed with 50  $\mu$ l of lysis buffer (20 mM Tris-HCl, pH 7.4, 150 mM NaCl, 5 mM MgCl<sub>2</sub>, and 1 mM DTT)

containing 1% Triton X-100, and then clarified by centrifugation with 20,000g at 4 °C for 10 min. Nascent peptides were labelled with 5  $\mu$ M Alexa Fluor 488 Azide (ThermoFisher Scientific) by a Click-it Cell Reaction Buffer Kit (ThermoFisher Scientific) according to the manufacturer's instructions and run on SDS-PAGE. Images were acquired by FluorChem R imaging system (ProteinSimple) and quantified by AlphaView (ProteinSimple).

**DNA constructs.** DNA fragments containing 5' UTRs sequences, listed below, were inserted between T7 promoter and ORF of *Renilla* luciferase (hRluc) in psiCHECK2 (Promega). We cloned exactly the same sequence of G-quadruplex and its control sequence used in ref. 5. These plasmids were digested by NotI and used as *in vitro* transcription template.

PTGES3 (uc001slu.4): GCCGCCCGCCTCACCACCCCTCGTT  
TGCACGCACGCATGTTCTTCTCCGTCCTCGCGCCCTTTTCTACTACT  
TTCTCTTCTCCCCGACCGGAGGAGCCGCTCTTCCGCGCGGTGCATT  
TGGGGCCCGAGTTCGAGCCCGCGCTGCCCGCTCGCCTGAGGGAAG  
CGAGAAGAGGCGCGACCGGAGAGAAAAAGCGGAGTCGCCACCGGAG  
AGAAGTCGACTCCCTAGCAGCAGCCCGCCGACAGAGGCCCGCCAC  
CAGTTCGCGCTCCCCCTGCCCGTTTCA.

EIF2S3 (uc004dbc.3): TTTCTTCTCTTTTGGCAAC.

HNRNPC (uc001vzy.3): AGGAATGGGGCGGGGACTAGGCCTT  
CGCTCGGCGCAGAGGAGACTCGGGGGCCATTTTGTGAAGAGACGAA  
GACTGACCGGTGTGGCCCGTTCGCCACTCCAGCAGCAGCTCGGCT  
TCTTACGCAGAACCCGGAGTAGGAGACTCAGAATCGAATCTCTTCT  
CCCTCCCTTCTTGTGAGATTTTTTGTATCTTACGCTACATTTTCGGCT  
TTGTGAGAACTTACCATCAAACAG.

GPX1 (uc021wxw.1): CAGTTAAAAGGAGCGCGCTGCTGGCCTCCCTTA  
CAGTGCTGTTCGGGCGCTCCGCTGGCTTCTTGACAATTCGCC.

TMA7 (uc003cte.1): GGGGAAGCGCGCGTACGGCC.

KMT2A (uc001pta.3): CTGCTTCACTTACGGGGCGAAC.

HCV IRES: GCCAGCCCCCTGATGGGGCGCAGACTCCACCATGAATC  
ACTCCCCTGTGAGGAAGTACTGCTTTCACGCAGAAAGCGTCTAGCCATG  
CGGTAGTATGAGTGTGCTGCAGCTCCAGGACCCCTCCCGGGAG  
AGCCATAGTGTCTGGGAACCGGTGATACACCGGAATTGCCAGGAC  
GACCGGTCTTCTTGGAGTTACCCGCTCAATGCCTGGAGATTTGGG  
CGTGCCCCGCAAGACTGCTAGCCGAGTAGTGTGGGTCCGAAAGGC  
CTTGTGGTACTGCCTGATAGGGTGTTCGAGTGCCTCCGGGAGGTCTC  
GTAGACCTGCACCATGAGCAGCAATCTAAACCTCAAAGAAAAACCA  
AACGTAAC.

G-quadruplex: CTAGGTTGAAAGTACTTTGACGGCGGGCGGGTCAA  
TCTTACGGCGGGCGGACATAGATACGGCGGGCGGGTAGAACTA  
CGGCGGGCGGGATTAGAATAGTAA (where letters in bold type represent  
G-quadruplex-forming sequences).

Randomized control for G-quadruplex: CTAGGGCGCACGTACTT  
CGACAACGTACGCTTACGCTTCCAACGTACGCTACAGCGATCCAA  
CGTCAGCGTCTGCGCTACAACGTACGCTATCCGCGTAGCACA.

CAA repeat: GAACAACAACAACAACAACAACAACAACAACAACAACA  
ACAACAACAACAACAACAACAACAACAACAACAACAACAACAACAACA

7 $\times$  AGAGAG motifs: GAAAGAGAGCAACAAGAGAGCAACAAGAGAG  
AGCAACAAGAGAGCAACAAGAGAGCAACAAGAGAGCAACAAGAGAG  
GAGCACC.

1 $\times$  AGAGAG left: GAAAGAGAGCAACAACAACAACAACAACAACA  
CAACAACAACAACAACAACAACAACAACAACAACAACAACAACAACA  
CAACACC.

1 $\times$  AGAGAG middle: GAACAACAACAACAACAACAACAACAACAACA  
CAACAAGAGAGCAACAACAACAACAACAACAACAACAACAACAACA  
CACC.

1 $\times$  AGAGAG right: GAACAACAACAACAACAACAACAACAACAACA  
CAACAACAACAACAACAACAACAACAACAACAACAACAACAAGAGAG  
GCACC.

Polio virus IRES: TAAAAACAGCTCTGGGGTGTACCACCCCG  
AGGCCACGTGGCGGTAGTACTCCGGTATTGCGGTACCCTGTACGC  
CTGTTTTATACCTCCCTCCCGTAACCTAGACGCAGAAAACCAAGTTCAA  
TAGAAGGGGGTACAAACCAGTACCACCAGCAACAAGCACTTCTGTTC  
CCCGGTGATGCTGATAGTACTGCTTGCCTGGTTGAAAGCGACGGATCCG  
TTATCCGCTTATGTACTTCGAGAAGCCAGTACCACCTCGGAATCTTCG  
ATGCGTTGCGCTCAGCACTAACCCAGTGTAGCTTAGGCTGATGAG  
TCTGGACATCCCTCACCGGTGACGGTGGTCCAGGCTGCGTGGCGGCC  
TACCTATGGCTAACGCCATGGGACGCTAGTTGTGAACAAGGTGTGAAG  
AGCCTATTGAGCTACATAAGAATCCTCCGGCCCTGAATGCGGCTAATC  
CCAACCTCGGAGCAGGTGGTACAAAACCAAGTATTGGCCTGTGTAAC  
GCGCAAGTCCGTGGCGGAACCGACTACTTTGGGTGTCCTGTTTCTT

TTATTTTATGTGGCTGCTTATGGTGACAATCACAGATTGTTATCATAAA  
CGGAATTGGATTGGCCATCCGGTGAAGTGAGACTCATTATCTATCTG  
TTTGCTGGATCCGCTCCATTGAGTGTGTTTACTCTAAGTACAATTTCAAC  
AGTTATTTCAATCAGACAATTGTATCATA.

Polio virus IRES 3× AGAGAG: TAAAAACAGCTCTGGGGTGTGA  
CCCACCCAGAGGCCACGTGGCGGTAGTACTCCGGTATTGCGGTACC  
CTTGTACGCTGTTTATACTCCCTCCCGTAACCTAGACGCACAAAACC  
AAGTTCAATAGAAGGGGTACAAACCAGTACCACCAAGCAACTT  
CTGTTTCCCGGTGATGTCGTATAGACTGCTTGGCGTGGTGAAGCGA  
CGGATCCGTTATCCGCTTATGACTTCGAGAAGCCAGTACCACCTCGG  
AATCTTCGATGCGTTGCGCTCAGCACTCAACCCAGAGGTGTAGCTTAG  
GCTGTAGTCTGGACATCCCTCACCCTGACGGTGACGGTCCAGGTCGG  
TTGGCGCTACCTATGGCTAACGCCATGGGACGCTAGTTGTGAACAA  
GGTGTGAAGAGCCTATTGAGCTACATAAGAATCCTCCGGCCCTGAAT  
GCGGCTAATCCCAACCTCGGAGCAGGTGGTGCACAAACCAGTGATTGG  
CCTGTGTAACGCGCAAGTCCGTGGCGGAACCGACTACTTTGGGTGTC  
CGTGTTCCTTTATTTATTTGCTGCTTATGGTGACAATCACAGATT  
GTTATCATAAAGCGAATTGGATTGGCCATCCGGTGAAGTGAGACTCAT  
TATCTATCTGTTTGGCTGGATCCGCTCCATTGAGAGAGTTACTCTAAGT  
AGAGAGTCAACAGTTATTAGAGAGACAATTGTATCATA.

The following DNA fragments, coding *Drosophila msl-2* 5' UTR and SBP, were amplified by PCR and used for *in vitro* transcription template.

uORF + CAACAA: TAATACGACTCACTATAGGGCAGCATAACCATTG  
TTGATGACTCGAGACCTCTCAAACGTAACCAACAACAAGCAGTGACA  
CCATGGACGAGAAAACACCGGCTGGCGGGGAGGCCAGTGGTGGAA  
GGGCTGGCAGGCGAGCTGGAACAGCTGCGGGCCAGACTGGAACACCA  
CCCCAGGGCCAGAGAGCCTAGCGGGGAGGAGACTACAAAGACC  
ATGACGGTATTATAAAGATCATGACATCGATTACAAGGATGACGATGA  
CAAGTGATTCTAGCGATCGCTCGAGCCGGGAATTCGTTTAAACCTA  
GAGCGGCC.

uORF + AGAGAG: TAATACGACTCACTATAGGGCAGCATAACCATTGTT  
GATGACTCGAGACCTCTCAAACGTAACCAACAAGAGGCGACGTCACAC  
CATGGACGAGAAAACACCGGCTGGCGGGGAGGCCAGTGGTGGAA  
GGCTGGCAGGCGAGCTGGAACAGCTGCGGGCCAGACTGGAACACCACC  
CCCAGGGCCAGAGAGCCTAGCGGGGAGGAGACTACAAAGACCAT  
GACGGTATTATAAAGATCATGACATCGATTACAAGGATGACGATGACA  
AGTGATTCTAGCGATCGCTCGAGCCGGGAATTCGTTTAAACCTAGA  
GCGGCC.

Reporter RNAs were *in vitro* transcribed, capped, and polyadenylated using a T7-Scribe Standard RNA IVT Kit, a ScriptCap m<sup>7</sup>G Capping System, a ScriptCap 2'-O-Methyltransferase Kit, and A-Plus Poly(A) Polymerase Tailing Kit (CELLSCRIPT). The capping reaction was skipped for polio virus IRES and polio virus IRES 3× AGAGAG reporters.

For the generation of stable cell-lines, PCR products containing CDS regions of *EIF4AI* mRNA and SBP amplified from cDNA from human adult normal brain (Invitrogen) and from pASW<sup>35</sup> (a gift from Y. Tomari), respectively, were inserted into HindIII site in pcDNA5/FRT/TO (Invitrogen) by Gibson assembly (NEB). P159Q, F163L, and Q195E mutations were introduced by site-directed mutagenesis.

For recombinant eIF4A protein expression, PCR products containing CDS regions of *EIF4AI* mRNA were inserted into pHM-GWA<sup>36</sup> to construct pHisMBP-eIF4A. VX<sub>4</sub>GKT (A82V) and D296A-T298K mutations were introduced by site-directed mutagenesis. His-tag, MBP-tag, tobacco etch virus protease cleavage site, and the N-terminal region of eIF4A (1–237) were cloned into pET-28a, to construct pHisMBP-eIF4A (1–237).

**Reporter assay in HEK 293 cells.** Transfections were performed in 24-well dishes with a TransIT-mRNA Transfection Kit (Mirus) according to the manufacturer's instructions, at half scale. Three hours after transfection, RocA was added to the medium, and 9 h after transfection cells were washed with PBS and lysed with Passive lysis buffer (Promega). The luciferase assay was performed with *Renilla*-Glo Luciferase Assay System (Promega) according to the manufacturer's instructions. Luminescence was detected with a GloMax-Multi Jr System (Promega).

For stable cell lines with SBP-tagged eIF4A and its mutants, HEK 293 Fip-In T-Rex cells were cultured for 4 days with 1 μg ml<sup>-1</sup> tetracycline before the experiments. Tetracycline was included in media during experiments.

**Quantitative PCR.** Cell lysate or *in vitro* translation reaction for luciferase assay was treated with 40 U ml<sup>-1</sup> TurboDNase for 10 min on ice, and then RNA was extracted by TRI Reagent (Sigma) and Direct-zol RNA MiniPrep (Zymo Research). Reverse transcriptions were performed with ProtoScript II (NEB) and random

primer mix (NEB) according to the manufacturer's instructions. Quantitative PCR (qPCR) was performed with Fast EvaGreen qPCR Mix (Biotium) in BioRad CFX96 Touch Real Time PCR Detection System (Bio-Rad) with oligonucleotides, 5'-TCGTCCATGCTGAGAGTGC-3', and 5'-CTAACCTCGCCCTTCTCCTT-3'. RNA from non-transfected cells or *in vitro* translation reaction without the addition of mRNAs was used as qPCR background.

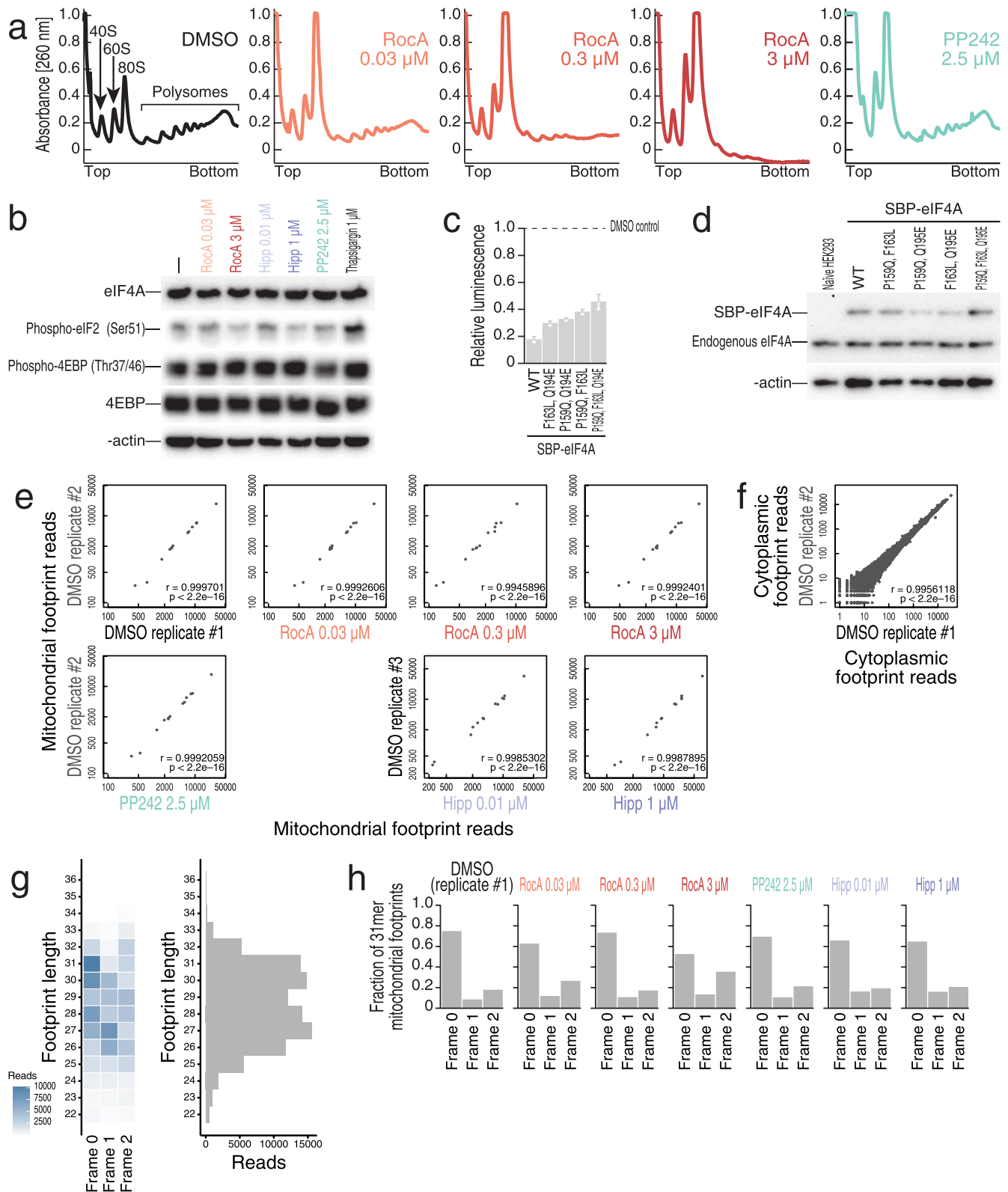
**Purification of recombinant eIF4A proteins.** Typically, BL21 Star (DE3) *Escherichia coli* cells (Invitrogen) transformed with pHisMBP-eIF4A, pHisMBP-eIF4A (VX<sub>4</sub>GKT), pHisMBP-eIF4A (D296A-T298K), or pHisMBP-eIF4A (1-237) in 1.5 L culture were cultivated to an absorbance at 600 nm,  $A_{600\text{ nm}}$ , of 0.5 at 37 °C with 50 μg ml<sup>-1</sup> kanamycin and then grown at 16 °C overnight with 1 mM IPTG. The cell pellets were resuspended in His buffer (20 mM HEPES-NaOH, pH 7.5, 500 mM NaCl, 10 mM imidazole, 10 mM β-mercaptoethanol) with 0.5% NP-40, sonicated, and centrifuged at 35,000g for 20 min. The supernatant was incubated with 1.5 ml bed volume of Ni-NTA Superflow (Qiagen) for 1 h. The beads were loaded on a gravity column and washed with His buffer containing 1 M NaCl. The proteins were eluted with 50 mM Na-phosphate buffer, pH 7.5, 500 mM NaCl, 100 mM Na<sub>2</sub>SO<sub>4</sub>, 250 mM imidazole, 10 mM β-mercaptoethanol, treated with tobacco etch virus protease overnight, dialysed to 20 mM HEPES-NaOH, pH 7.0, 150 mM NaCl, 0.5 mM TCEP, and 10% glycerol, and loaded on MBPTrap HP 5 ml (GE Healthcare). The flow-through fractions were collected, concentrated with Amicon Ultra 10kDa (Millipore), and loaded onto a HiLoad 16/600 Superdex 75 prep grade column (GE Healthcare) equilibrated with 20 mM HEPES-NaOH, pH 7.5, 150 mM NaCl, 0.5 mM TCEP. The peak fractions were collected, concentrated with Amicon Ultra 10kDa (Millipore), mixed with 0.25 volumes of 80% glycerol, shock-frozen in liquid nitrogen, and stored at -80 °C. All purification steps were performed at 4 °C. Column chromatography was performed using an AKTA purifier (GE Healthcare).

**Pulldown assay.** The lysate of *E. coli* cells expressing eIF4A wild type (WT) or eIF4A D296A-T298K proteins from 1 ml culture was prepared as described in 'Purification of recombinant eIF4A proteins' and incubated with 10 μl of HisPur Ni-NTA Magnetic Beads (Thermo Scientific) at 4 °C for 30 min. The beads were washed five times with His buffer containing 1 M NaCl, rinsed once with 20 mM HEPES-NaOH, pH 7.5, 10 mM NaCl, 10 mM imidazole, 10 mM β-mercaptoethanol, and incubated with RRL (Promega) at 25 °C for 30 min. After five washes with His buffer, the proteins were eluted with SDS sample buffer.

**ATP crosslinking assay.** Recombinant eIF4A WT and VX<sub>4</sub>GKT (10 μM) was incubated with 1 μM [<sup>32</sup>P]-ATP (3,000 Ci mmol<sup>-1</sup>, Perkin Elmer) in 30 mM HEPES-KOH, pH 7.3 (Fisher Scientific), 100 mM KOAc, 5 mM Mg(OAc)<sub>2</sub>, and 1 mM DTT in 20 μl reaction at 37 °C for 15 min. The reactions were exposed to 1500 mJ cm<sup>-2</sup> using UV<sub>254 nm</sub> (CL-1000, UVP) at a distance of 2 cm from the lamp on ice and run on SDS-PAGE. The images were acquired by Typhoon TRIO (Amersham Biosciences).

**Western blotting.** Anti-eIF4AI (2490, Cell signaling) (1:1,000), anti-phospho-eIF2α (Ser51) (D9G8 3398, Cell Signaling) (1:1,000), anti-4E-BP1 (9452, Cell Signaling) (1:2,000), anti-phospho-4EBP (Thr37/46) (236B4 2855, Cell Signaling) (1:2,000), anti-β-actin (ab20272, Abcam) (1:1,000), anti-eIF4E (9742, Cell Signaling) (1:1,000), anti-eIF4G (2498, Cell Signaling) (1:1,000), and anti-SBP-tag (SB19-C4 sc-101595, Santa Cruz Biotechnology) (1:1,000) were used as primary antibodies. Chemiluminescence was induced by Pierce ECL Western Blotting Substrate (Thermo Scientific) and images were acquired by a FluorChem R imaging system (ProteinSimple).

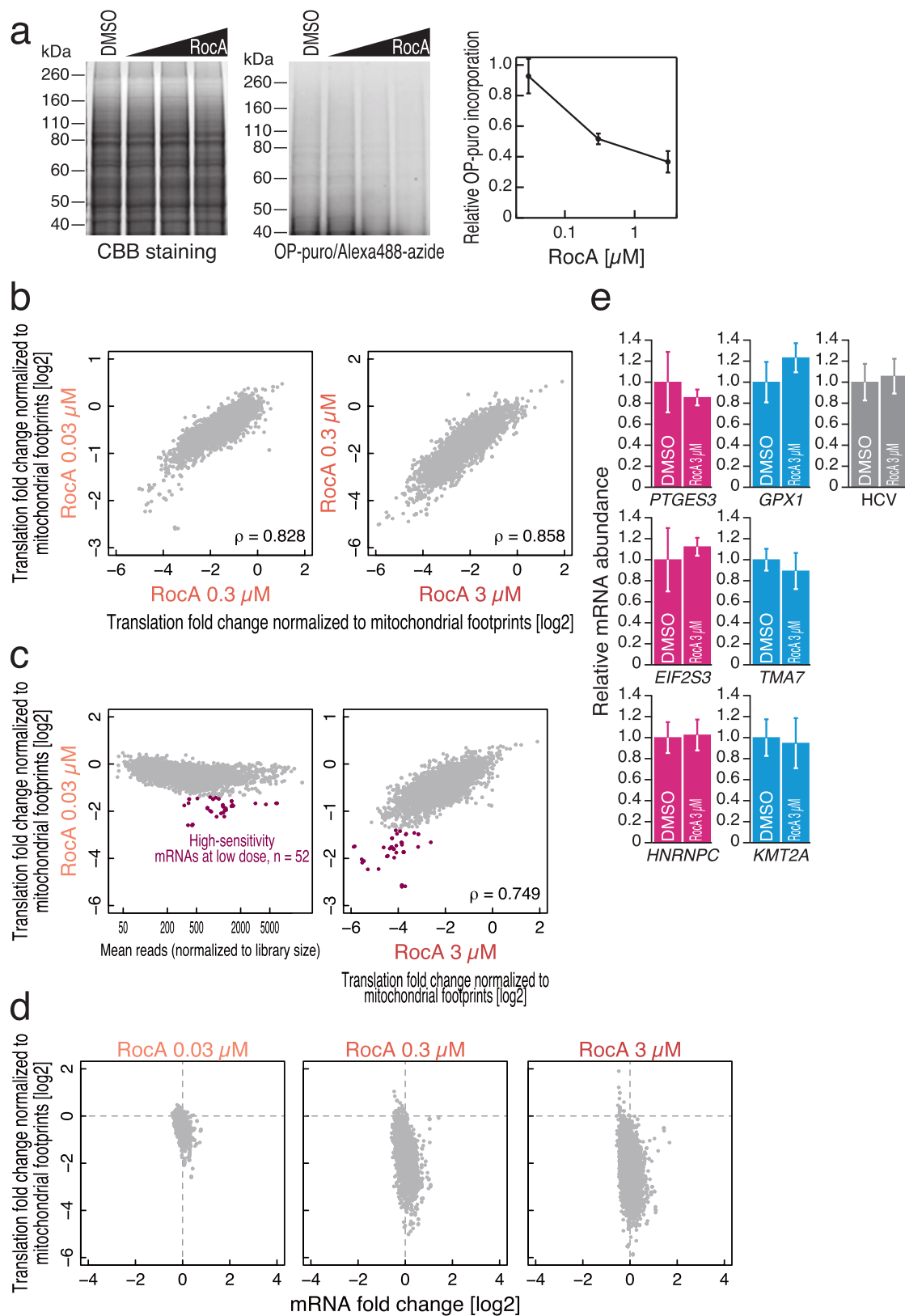
- Ingolia, N. T., Brar, G. A., Rouskin, S., McGeachy, A. M. & Weissman, J. S. The ribosome profiling strategy for monitoring translation *in vivo* by deep sequencing of ribosome-protected mRNA fragments. *Nature Protocols* **7**, 1534–1550 (2012).
- Anders, S. & Huber, W. Differential expression analysis for sequence count data. *Genome Biol.* **11**, R106 (2010).
- Lorenz, R. *et al.* ViennaRNA Package 2.0. *Algorithms Mol. Biol.* **6**, 26 (2011).
- Dmitriev, S. E., Pisarev, A. V., Rubtsova, M. P., Dunaevsky, Y. E. & Shatsky, I. N. Conversion of 48S translation preinitiation complexes into 80S initiation complexes as revealed by toeprinting. *FEBS Lett.* **533**, 99–104 (2003).
- Iwasaki, S. *et al.* Hsc70/Hsp90 chaperone machinery mediates ATP-dependent RISC loading of small RNA duplexes. *Mol. Cell* **39**, 292–299 (2010).
- Busso, D., Delagoutte-Busso, B. & Moras, D. Construction of a set Gateway-based destination vectors for high-throughput cloning and expression screening in *Escherichia coli*. *Anal. Biochem.* **343**, 313–321 (2005).
- Galicía-Vázquez, G., Cencic, R., Robert, F., Agenor, A. Q. & Pelletier, J. A cellular response linking eIF4AI activity to eIF4AI transcription. *RNA* **18**, 1373–1384 (2012).



**Extended Data Figure 1 | RocA represses translation, targeting to eIF4A.** **a**, Polysome profiling experiments with RocA and PP242 treatments. RocA disrupts polysomes dose-dependently. **b**, Western blot of phospho-eIF2 $\alpha$  and phospho-4EBP shows that effect of RocA is independent of known translation control targeting to eIFs. Phosphorylation of eIF2 $\alpha$  and dephosphorylation of 4EBP were induced by thapsigargin and PP242, respectively. **c**, **d**, Luciferase reporter assay possessing *PTGES3* 5' UTR (Fig. 1c) with exogenous expression of WT or RocA-resistant eIF4A mutants (c) and western blot of endogenous and exogenous eIF4A (d). eIF4A is the main molecular target of RocA. Data represent mean and s.d. ( $n=3$ ). **e**, **f**, Correlation of sum of the

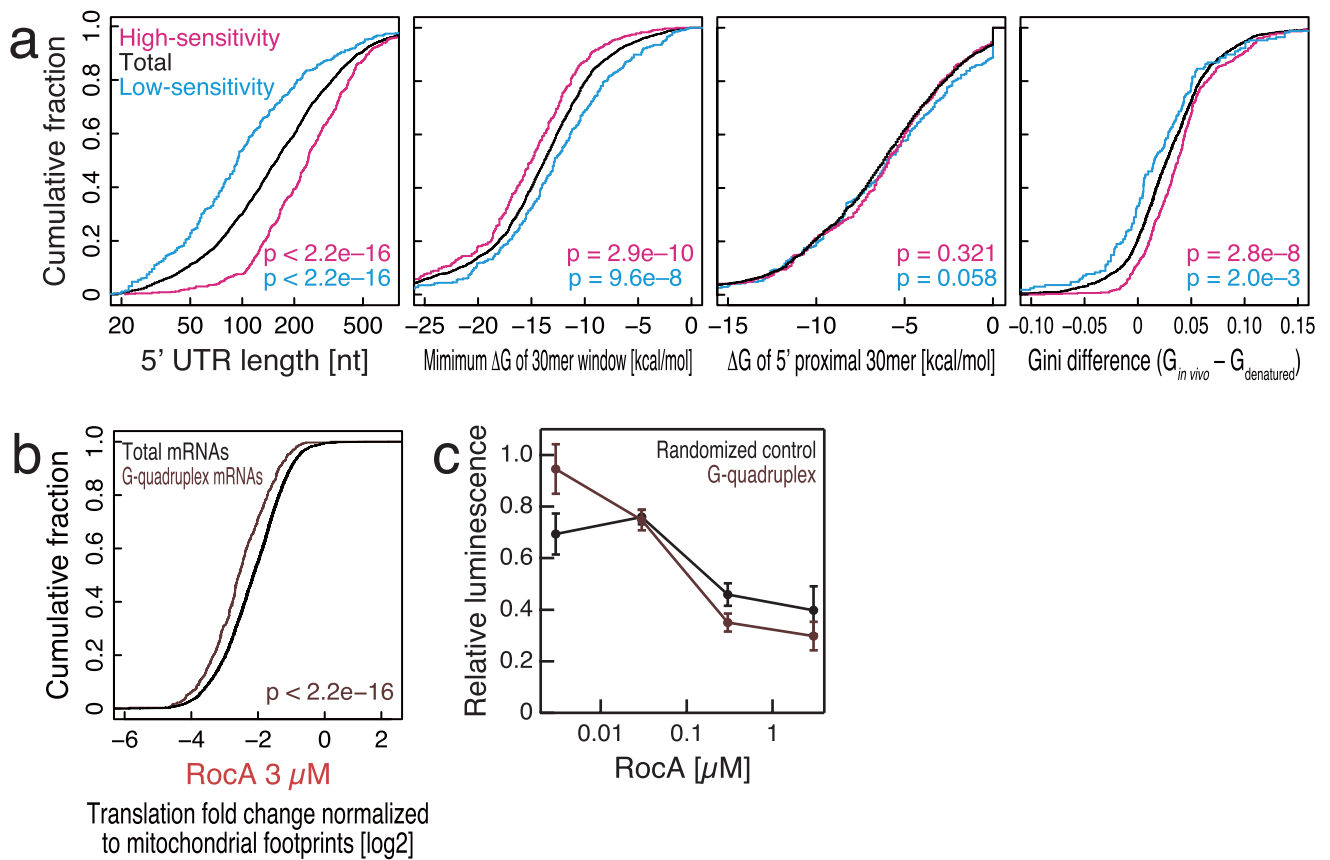
footprint reads to 13 mitochondrial mRNAs among different conditions (e) and correlation of sum of the footprint reads from cytoplasmic ribosomes to each transcript between biological replicates (f). Symbol  $r$  is Pearson's correlation.  $P$  value is calculated by Student's  $t$ -test. **g**, **h**, Tile plot of codon periodicity along length of mitochondria footprints (g, left) and mitochondria footprint length distribution (g, right) and codon periodicities of 31-nt mitochondrial footprints among different conditions (h). Footprints with 31-nt length showed most homogenous codon periodicity, and this periodicity was retained with RocA treatment, showing that mitochondrial ribosome translates even in high doses of RocA.





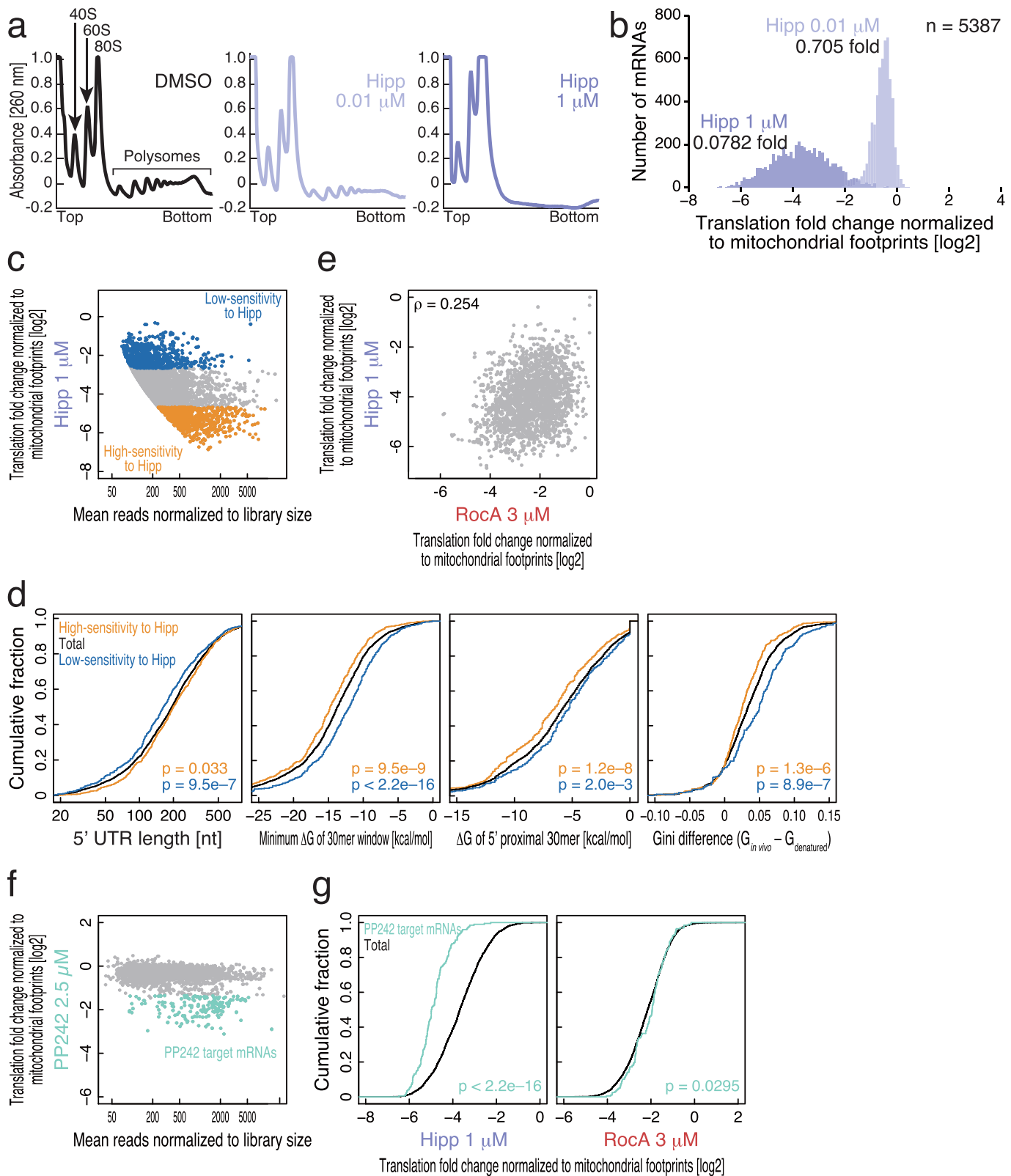
**Extended Data Figure 2 | RocA represses translation without mRNA degradation.** **a**, Metabolic labelling of nascent peptides with OP-puro. The OP-puro incorporated nascent peptides were visualized by Click reaction with Alexa Fluor 488 Azide (middle) and quantified (right). Data represent mean and s.d. ( $n = 3$ ). **b**, Correlation of translation -fold change among different concentrations of RocA treatments. **c**, MA plot of mean footprint reads between 0.03  $\mu\text{M}$  RocA treatment and non-treatment normalized to

library sizes to footprints -fold change by 0.03  $\mu\text{M}$  RocA treatment (left) and the correlation of translation -fold change between 0.03 and 3  $\mu\text{M}$  of RocA treatments (right), highlighting high-sensitivity mRNAs at 0.03  $\mu\text{M}$  RocA treatment. **d**, Scatter plots of footprint -fold change normalized to mitochondrial footprints and mRNA -fold change by RocA treatments. RocA represses translation without significant mRNA change. **e**, qPCR from the samples of Fig. 1c. Data represent mean and s.d. ( $n = 3$ ).



**Extended Data Figure 3 | Secondary structure in 5' UTR is not strong determinant of RocA sensitivity.** **a**, Cumulative fractions along length of 5' UTR, minimum  $\Delta G$  among all 30-mer windows along a 5' UTR,  $\Delta G$  in cap-proximal region (30 nt) of 5' UTR, and Gini difference are plotted to total, RocA high-sensitivity, and RocA low-sensitivity mRNAs. Significance is calculated by Mann–Whitney  $U$ -test. **b**, Cumulative fractions along translation -fold change by RocA are plotted to total

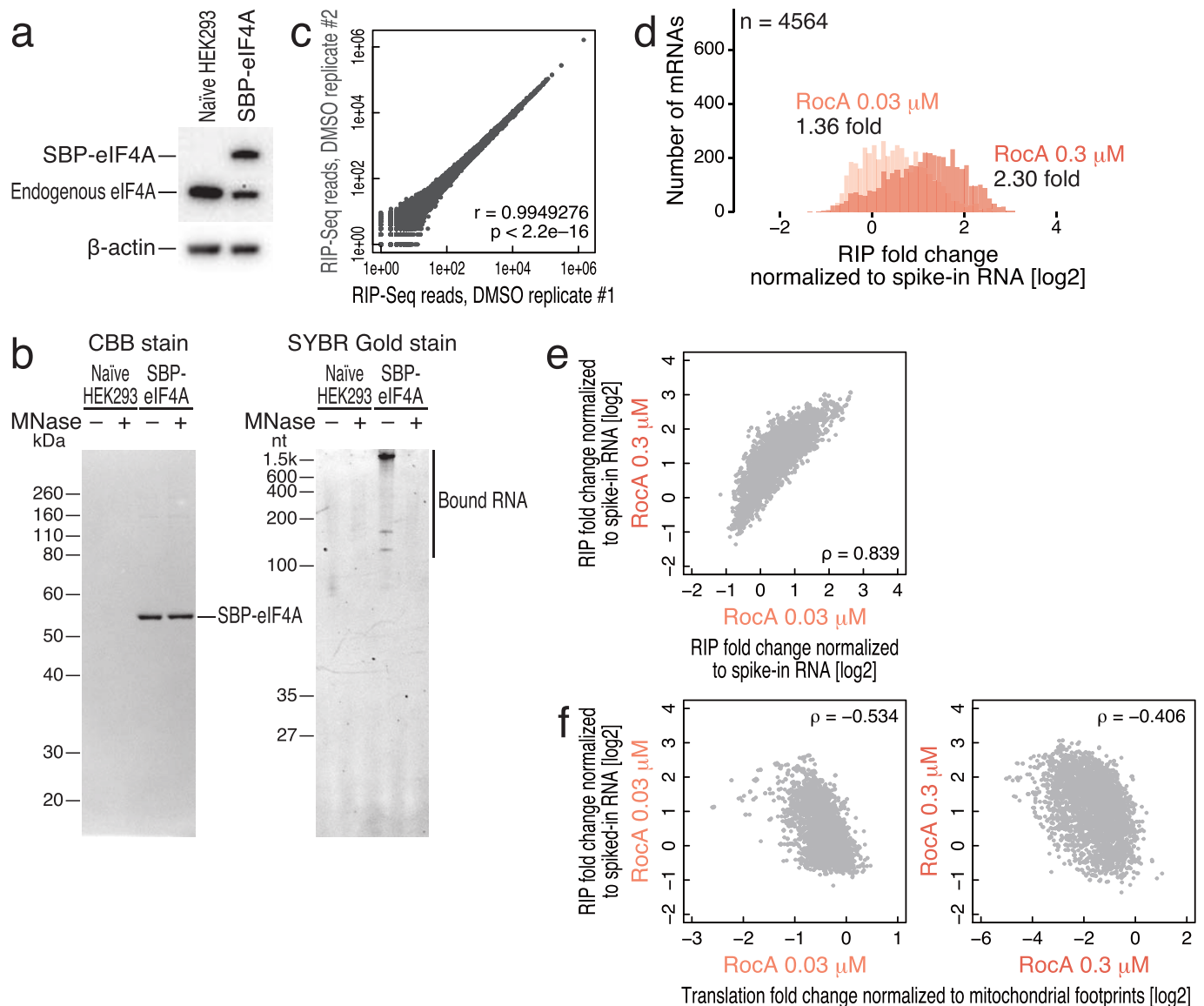
mRNAs and mRNAs with predicted G-quadruplexes in 5' UTRs. Significance is calculated by Mann–Whitney  $U$ -test. The impact of presence of G-quadruplex in 5' UTR is modest in RocA sensitivity. **c**, The 5' UTRs with G-quadruplexes and randomized control sequence were fused to *Renilla* luciferase and these reporter mRNAs were transfected before treatment with RocA as indicated. Data represent mean and s.d. ( $n = 3$ ). G-quadruplex does not show the prominent RocA sensitivity.



#### Extended Data Figure 4 | Characterization of translational inhibition

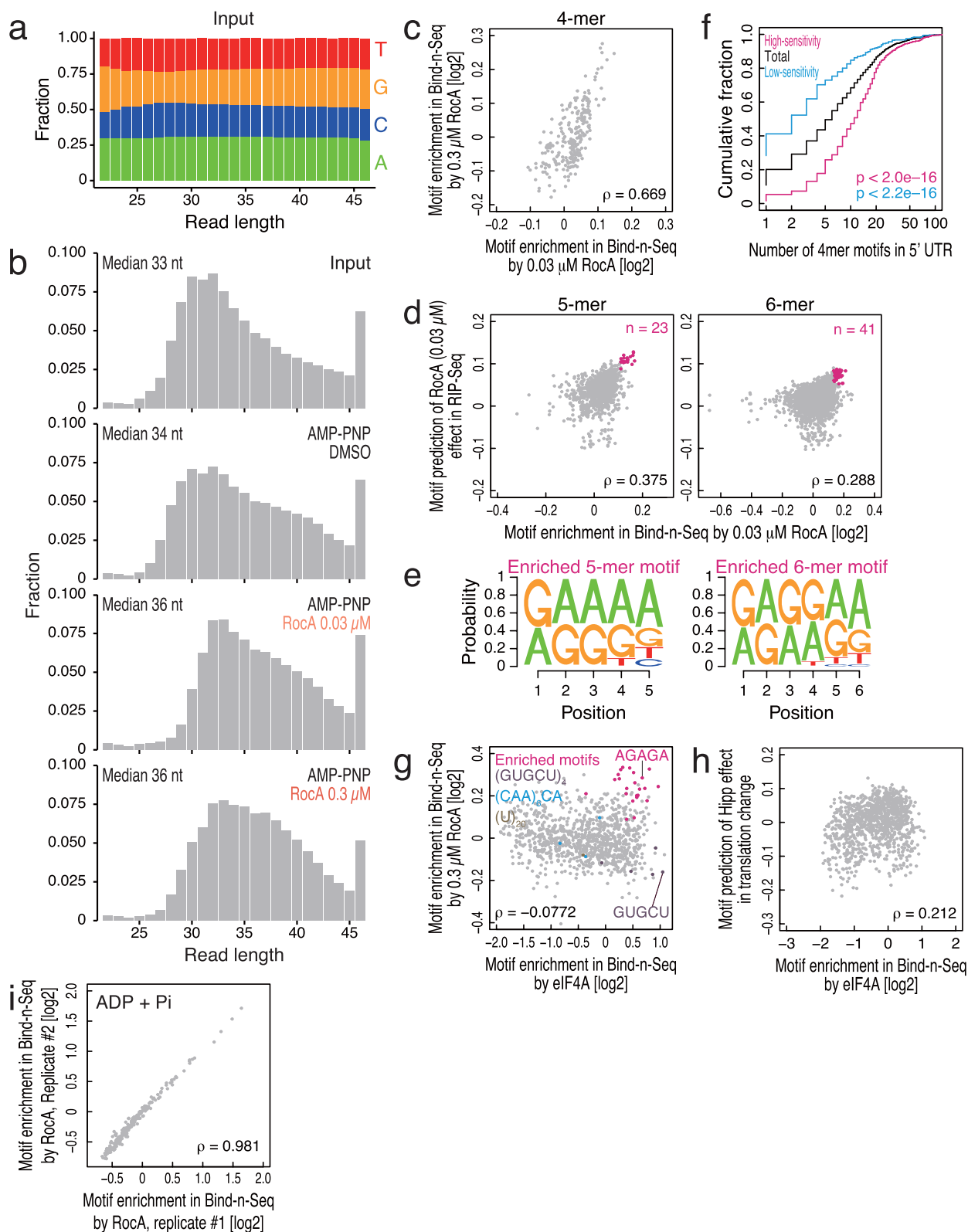
by Hippuristanol and PP242. **a**, Polysome profiling experiments with Hipp treatments. Hipp disrupts polysomes dose-dependently. **b**, Histograms of number of transcripts along footprints -fold change with 0.01 and 1  $\mu\text{M}$  Hipp treatment compared with non-treatment, normalized to mitochondrial footprints. Median -fold change is shown. Bin width is 0.1. **c**, MA plot of mean footprint reads between 1  $\mu\text{M}$  Hipp treatment and non-treatment normalized to library sizes to translation -fold change by 1  $\mu\text{M}$  Hipp treatment, highlighting high-sensitivity and low-sensitivity mRNAs. **d**, Cumulative fractions along length of 5' UTR, minimum  $\Delta G$

among all 30-mer windows along a 5' UTR,  $\Delta G$  in cap-proximal region (30 nt) of 5' UTR, and Gini difference are plotted to total, Hipp high-sensitivity, and Hipp low-sensitivity mRNAs. Significance is calculated by Mann-Whitney  $U$ -test. **e**, Translation -fold changes by RocA and Hipp are modestly correlated. **f**, MA plot of mean footprint reads between 2.5  $\mu\text{M}$  PP242 treatment and non-treatment normalized to library sizes to translation -fold change by PP242 treatment, highlighting PP242 target mRNAs. **g**, Cumulative distributions of translation -fold change caused by RocA and Hipp treatment are plotted for total and PP242-target mRNAs. Significance is calculated by Mann-Whitney  $U$ -test.



**Extended Data Figure 5 | Purification of SBP-tagged eIF4A and co-purified RNA from HEK 293 cells.** **a**, Western blot of exogenous SBP-eIF4A and endogenous eIF4A in tetracycline-inducible stable cell line. Expression of physiological levels of the tagged allele attenuated endogenous eIF4A expression but preserved overall eIF4A levels, probably reflecting the same feedback loop previously reported between eIF4A1 and eIF4A11<sup>37</sup>. **b**, CBB staining of purified SBP-eIF4A and SYBR Gold staining of purified RNA bound to SBP-eIF4A with or without micrococcal nuclease (MNase). **c**, Correlation of sum of the mRNA

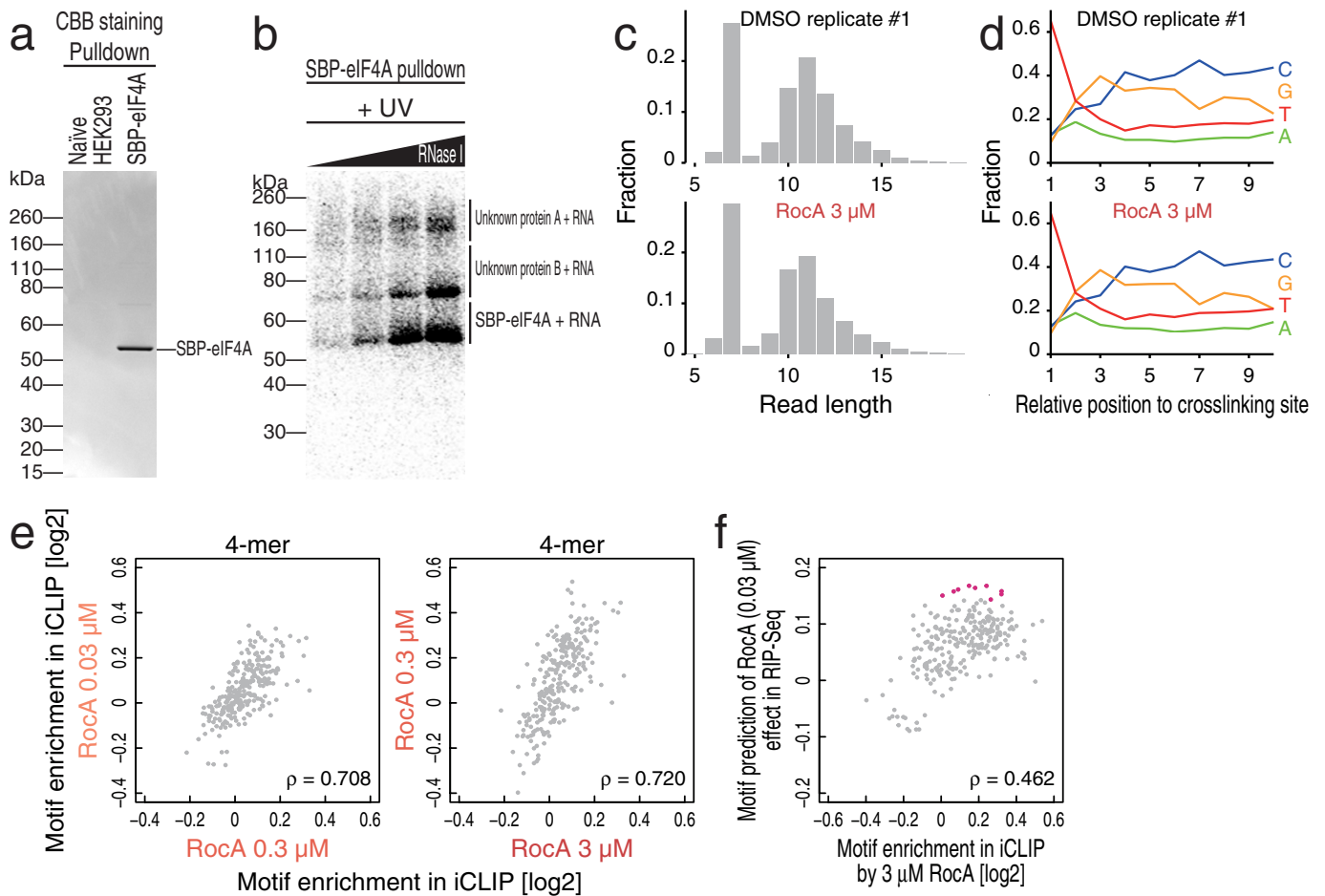
fragment reads of each transcript between biological replicates of RIP-seq. *P* value is calculated by Student's *t*-test. **d**, Histogram of the number of transcripts along RNA/eIF4A interaction -fold change by RIP-seq when cells are treated with 0.03 or 0.3 μM RocA normalized to spiked-in RNA. Data present the same mRNAs analysed in Fig. 1a. Median -fold change is shown. Bin width is 0.1. **e**, Correlation of RIP -fold change between different concentration of RocA treatments. **f**, Correlation of translation -fold change to RIP -fold change with the same concentration of RocA treatment.



### Extended Data Figure 6 | Motif enrichment by Bind-n-Seq.

**a**, Nucleotide composition in each length of reads in input RNAs for Bind-n-Seq. Input RNAs are random in entire read length. **b**, Length distribution of reads from Bind-n-Seq. RNAs bound to eIF4A showed longer length distribution, indicating that eIF4A has preference for longer RNAs. **c**, Correlations of tetramer motif enrichment in Bind-n-Seq by 0.03  $\mu\text{M}$  RocA treatment to that by 0.3  $\mu\text{M}$  RocA treatment. **d**, Correlations between pentamer and hexamer motif enrichment in Bind-n-Seq by 0.03  $\mu\text{M}$  RocA treatment and motif prediction of 0.03  $\mu\text{M}$  RocA effect in RIP-seq. **e**, Highest-scoring pentamer and hexamer motifs in Bind-n-Seq and RIP-seq. **f**, Cumulative fractions along number of tetramer motifs (Fig. 2b)

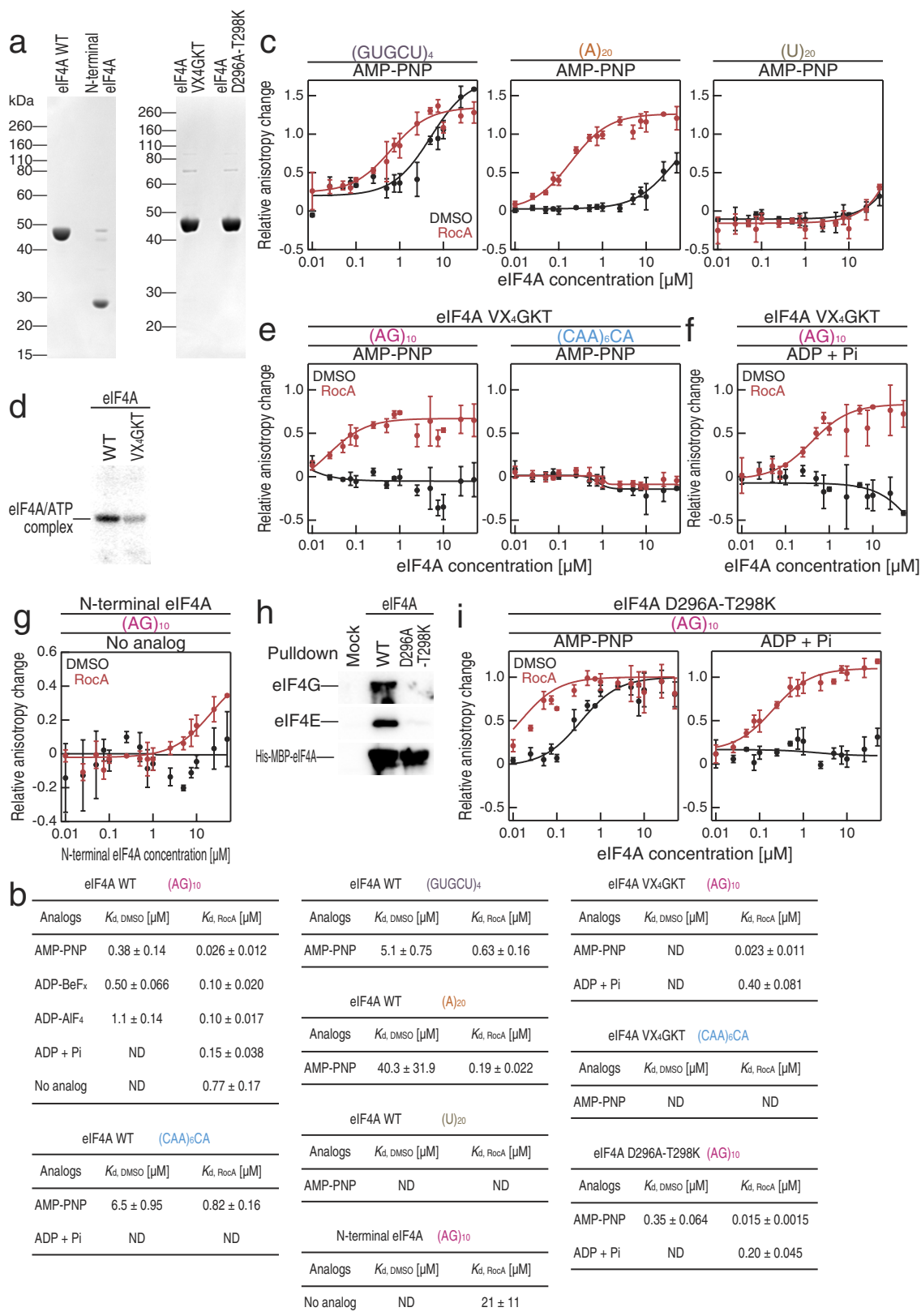
in 5' UTR are plotted to total, RocA high-sensitivity, and RocA low-sensitivity mRNAs. Significance is calculated by Mann-Whitney  $U$ -test. **g**, Correlations of Bind-n-Seq motif enrichment (pentamer) by eIF4A to that by 0.03  $\mu\text{M}$  RocA treatment. The motifs appearing in RNAs used in Extended Data Fig. 8 are highlighted. **h**, Correlation of Bind-n-Seq motif enrichment (pentamer) by eIF4A to motif prediction of Hipp effect in translation change, which is defined as Spearman's correlation of motif number in 5' UTR to translation -fold change by Hipp. mRNAs with high-affinity motif to eIF4A in 5' UTR are resistant to Hipp treatment. **i**, The correlation between enriched motifs of replicates in Bind-n-Seq with ADP + Pi.



#### Extended Data Figure 7 | Characterization of iCLIP data.

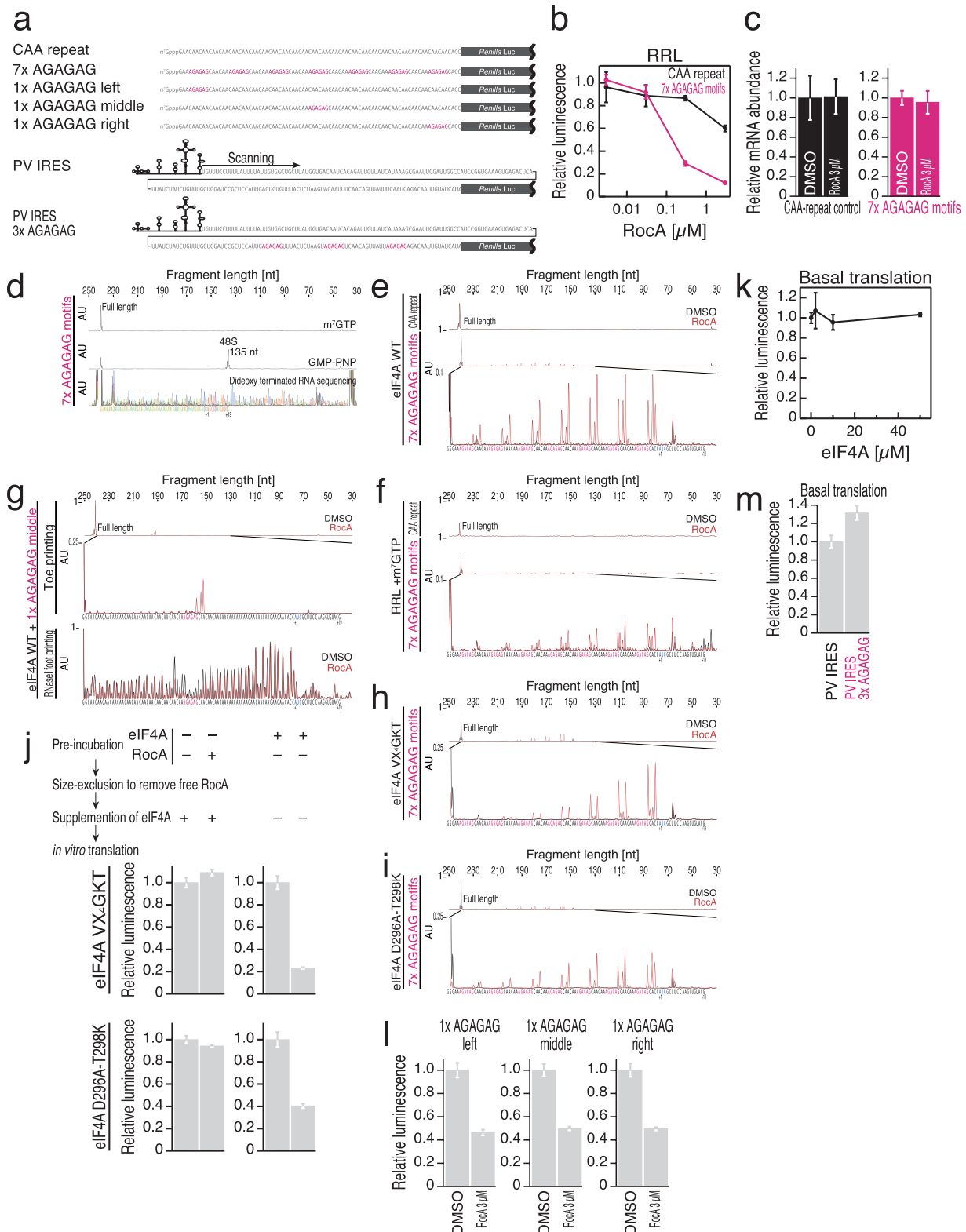
**a**, CBB staining of purified SBP-eIF4A protein in iCLIP procedure. **b**, Visualization of RNA-crosslinked with SBP-eIF4A and unknown proteins by  $^{32}$ P labelling of RNA. We avoided the contamination of RNAs cross-linked to the additional, co-purifying, unknown proteins. **c**, Distribution of read length in iCLIP libraries. Avoidance of contaminating RNAs restricted us to short RNAs, which probably

correspond to the region of RNA physically protected by eIF4A binding, or footprint. **d**, Nucleotide bias along the reads in iCLIP libraries. The crosslinking bias for U may underestimate the preference for polypurine motifs. **e**, Correlations of iCLIP motif enrichment (tetramer) by different RocA concentrations. **f**, Correlations of iCLIP motif enrichment (tetramer) by 3  $\mu$ M RocA and motif prediction of 0.03  $\mu$ M RocA effect in RIP-seq. The motifs shown in Fig. 2a are highlighted.



**Extended Data Figure 8 | eIF4A/RNA affinity measured by fluorescence polarization.** **a**, CBB staining of recombinant proteins used in this study. **b**, Summary of  $K_d$  between RNA and eIF4A among the conditions assayed. **c**, **e–g**, **i**, Direct measurement of the eIF4A/RNA affinity by fluorescence polarization for eIF4A WT, eIF4A (VX<sub>4</sub>GKT), or eIF4A (D296A–T298K)

and 5' FAM-labelled RNAs in the presence or absence of RocA. Data represent mean and s.d. ( $n = 3$ ). **d**, ATP crosslinking assay with eIF4A WT and eIF4A (VX<sub>4</sub>GKT). **h**, Pull-down assay with His-MBP-eIF4A expressed in *E. coli* and eIF4E/G in RRL.

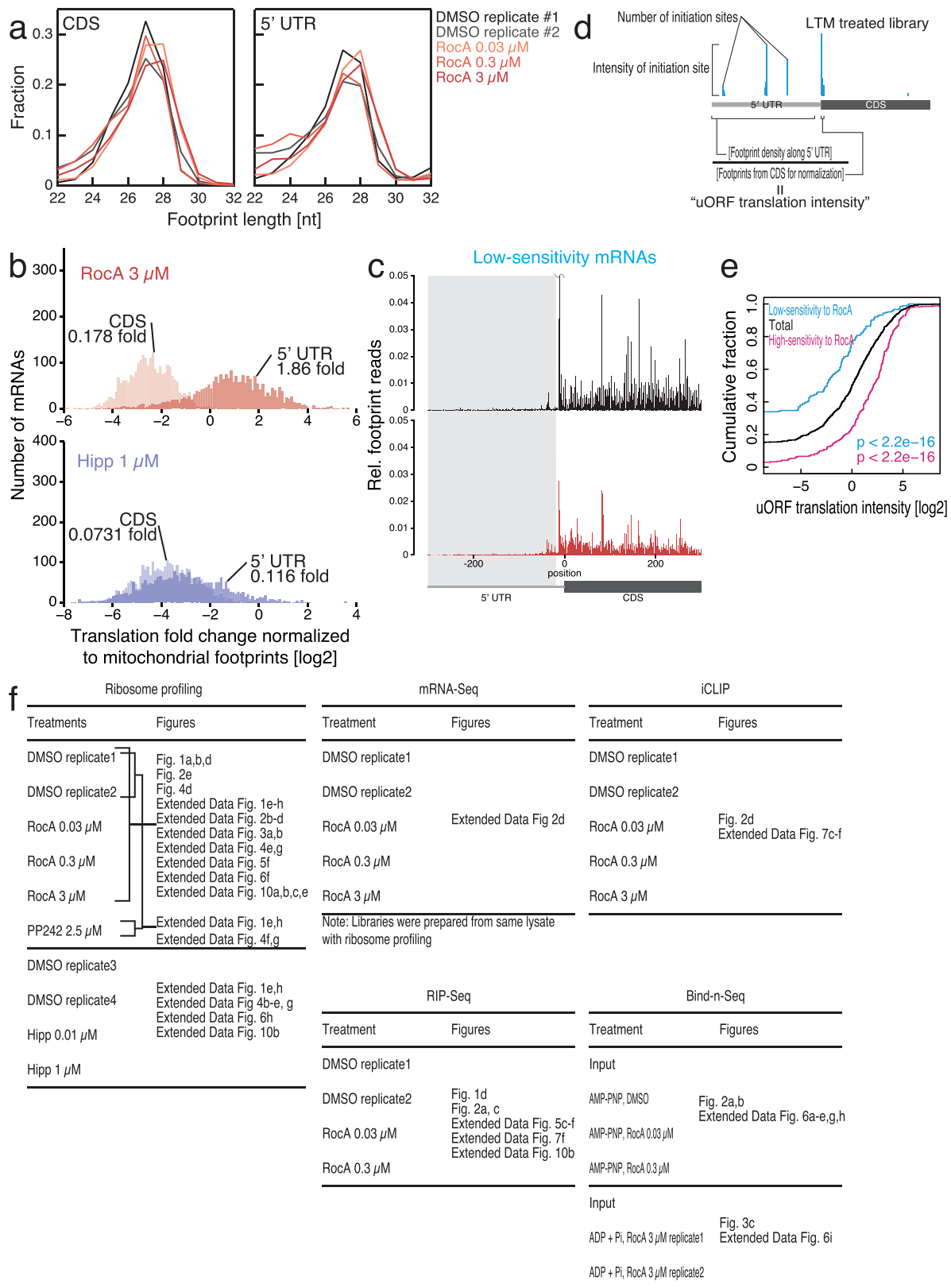


### Extended Data Figure 9 | Characterization of toeprinting assay.

**a**, Diagram of the reporters used in this study. **b**, **c**, *In vitro* translation in RRL with mRNAs containing seven polypurine motif (AGAGAG) insertions (**b**) and qPCR from the samples (**c**). **d**, Dideoxy-terminated sequencing of RNA by reverse transcription verified the toeprinting product length terminated by 48S ribosomes. **e**, Ribosome toeprinting assay performed in RRL in the presence of m<sup>7</sup>-GTP in the presence or absence of 3  $\mu$ M RocA treatment. **f**, Toeprinting assay using 10  $\mu$ M recombinant eIF4A in the presence or absence of 10  $\mu$ M RocA treatment. **g**, Toeprinting assay (top) and RNase I footprinting assay (bottom) using 10  $\mu$ M recombinant eIF4A with mRNA containing one AGAGAG motif at the middle in the presence or absence of 10  $\mu$ M RocA treatment.

**h**, **i**, Toeprinting assay using 10  $\mu$ M recombinant eIF4A (VX<sub>4</sub>GKT) or (D296A-T298K) with mRNA containing seven AGAGAG motifs in the presence or absence of 10  $\mu$ M RocA treatment. **j**, Pre-formation of the complex with RocA and eIF4A (VX<sub>4</sub>GKT) or (D296A-T298K) on the mRNA bearing seven polypurine motifs represses the translation from the mRNA in RRL. **k**, Basal translation level from mRNA containing seven AGAGAG motifs with the supplementation of recombinant eIF4A. **l**, *In vitro* translation in RRL with mRNAs with a single polypurine motif (AGAGAG) insertion at the different positions in 5' UTR. **m**, Basal translation level from mRNAs bearing polio virus IRES and polio virus IRES with three AGAGAG motifs. In **b**, **c**, and **h**–**j**, data represent mean and s.d. ( $n = 3$ ).





**Extended Data Figure 10 | The 5' UTR footprints accumulated in RocA treatments come from uORFs.** **a**, The distributions of specific footprint length, which is a hallmark of 80S ribosomes<sup>8</sup>, from CDS and 5' UTR are indistinguishable. **b**, The change in ribosome footprint counts for 5' UTRs and CDSs when cells are treated with 3  $\mu\text{M}$  RocA or 1  $\mu\text{M}$  Hipp compared with non-treatment, normalized to mitochondrial footprints. Median -fold change is shown. Bin width is 0.1. Analysis is restricted to mRNAs bearing footprints in the 5' UTR in the non-treatment condition. **c**, Meta-gene

analysis of low-sensitivity transcripts to RocA. Reads are normalized to the sum of mitochondrial footprints reads. **d**, The illustration of the definition of uORF translation intensity. **e**, Transcripts sensitive to RocA contain more active uORFs, as measured by cumulative distributions of the uORF translation intensity **c**. Significance is calculated by Mann-Whitney *U*-test. **f**, The summary of deep sequencing-based approaches used in this study and corresponding figures.